Russian Chemical Reviews **82** (9) 815–834 (2013) © 2013 Russian Academy of Sciences and Turpion Ltd

DOI 10.1070/RC2013v082n09ABEH004357

Activation of solid-phase processes by radiation of gas-discharge lamps

V M Ievlev

Contents

I.	Introduction	815
II.	Synthesis of metal silicide films	817
III.	Recrystallization of thin films	823
IV.	Nanocrystallization of amorphous structures	825
V.	Synthesis of oxide, nitride and carbide films	827
VI.	Conclusion	831

Abstract. Results of studies on application of broadband radiation of gas-discharge lamps for activation of solid-phase processes including the synthesis of thin films, nanocrystallization of amorphous structures, recrystallization and modification of thin films formed by various methods are analyzed and generalized. Compared to conventional thermal processing, the effect of photon treatment manifests itself in acceleration of processes, higher degree of dispersion of structures formed and in reduction of temperature thresholds for the phase formation. Prospects for application of photon activation in industrial processes are discussed. The bibliography includes 142 references.

I. Introduction

Since the 1980s, a number of solid-phase processes used in technology of semiconductor devices have been activated by rapid photon treatment with broadband radiation of power pulsed gas-discharge lamps instead of traditionally used thermal processing† because of pronounced thermal effect of the interaction of light with some solids (*e.g.*, silicon and gallium arsenide crystals).

Rapid photon treatment by illumination with light of gas-discharge lamps has become the main method on going to sub-micrometre technologies in microelectronics. The range of practically implemented and currently studied processes activated by illumination with light of halogen or xenon lamps is rather wide. It includes, *e.g.*, the synthesis of metal silicide films,[1–5] bilayer $TiN/TiSi_2$ films,[6] oxide films,[7,8] annealing of implanted layers,[9–13] solid-phase crystallization of amorphous silicon layers and formation of silicon/dielectric heterostructures,[14–19] formation of Ohmic contacts,[20,21] diffusion[22] and changes in the charge carrier mobility,[19,22–25] formation of bulk recombination sites,[24] shallow and ultrashallow n^+-p^- and p^+-n^- junctions (Refs 26 and 27), intrinsic gettering of impurities in single-crystalline silicon wafers,[28,29] surface cleaning, *etc.*[30]

To prevent the development of undesired processes in some technologies of solid-state electronics (*e.g.*, the formation of ultrashallow junctions requires minimization of the possibility of dopant redistribution and oxidation of the open silicon surface), short-term annealing accompanied by heating to rather high temperatures is used.

Rapid photon treatment is also efficient in the synthesis of oxide films (*e.g.*, rutile films[31]) in fabrication of random access memory devices, optically transparent conductive oxides with high Q-factor values,[32,33] metal nitrides,[34–36] silicon nitrides,[37,38] in modification of the structure and, therefore, properties of films prepared in by various methods,[39–43] for creation and size control of quantum dots in oxide films,[44,45] for the formation of p–n junctions in the course of photostimulated doping as a step in molecular-beam epitaxy of multilayer heterostructures based on, *e.g.*, CdTe,[46] and for creation of hydroxyapatite nucleation sites in solution methods of apatite growth on metallic implants (formation of OH groups on zirconia surface used as anode).[47] Photon treatment can also be utilized in the solid-phase synthesis of semiconductor films,[48] complex oxide films,[49–53] carbidization of refractory metal films[54] and single-crystalline silicon wafers,[55] nanostructuring and strengthening of amorphous alloy foils,[56–58] as well as in enhancement of adhesion of the hydroxyapatite coating to titanium.[59]

Practical implementation of photon treatment is based on the following features of the technique:

— broad emission spectrum (from 0.3 to 3.5 μm for halogen lamps[60] and from 0.17 to 1.2 μm for xenon lamps,

V M Ievlev Voronezh State University, pl. Universitetskaya 1, 394006 Voronezh, Russian Federation. Tel. (7-473) 220 87 35, e-mail: rnileme@mail.ru

Received 29 October 2012
Uspekhi Khimii **81** (9) 815–834 (2013); translated by A M Raevskyi

† The technique is also called Rapid Thermal Annealing (RTA) or Rapid Thermal Processing (RTP).

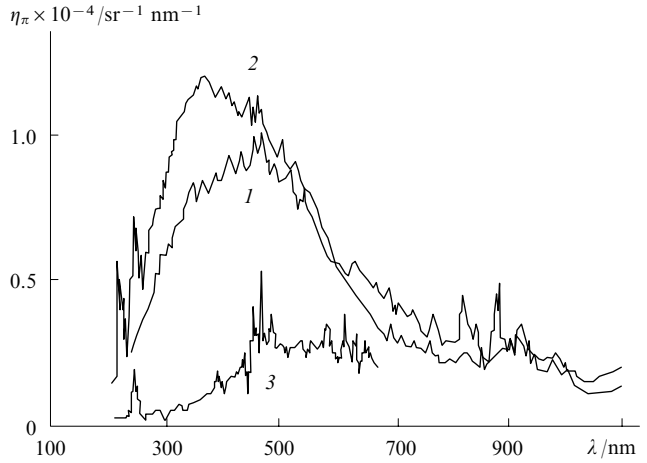


Figure 1. Spectral distribution of the efficiency of a xenon lamp over the unit solid angle.[61]
Specific discharge power/W m^{-3}: 1.1×10^{11} (*1*), 3.4×10^{11} (*2*) and 1.1×10^{8} (*3*).

see Fig. 1);[61,62] in the latter case, up to 90% of power output falls in the region from 0.17 to 0.3 μm,[25] which makes it possible to organize the response of different materials to irradiation taking into account their reflectance, absorption and transmission spectra;

— the possibility of processing various materials *in vacuo*, in air, as well as in inert and reactive gas atmospheres;

— the possibility of efficient processing of rather large surface areas and surfaces with developed morphology;

— the possibility of dosage of treatment duration (*e.g.*, the duration of a single illumination with light of a xenon lamp can vary from a few tenths of a second to a few seconds) and, consequently, radiation energy supplied to the sample;

— spatial localization of radiation;

— relatively high heating rate (from tens to hundreds of degrees per second[8,63]) and corresponding features of the kinetics of the processes being accelerated and the advantages over furnace processing; this makes it possible to exclude accompanying processes that are less temperature dependent;

— at pulse durations greater than 10^{-2} s, the heat balance conditions are met; this means that the thermal wave front reaches the back (nonirradiated) side of the sample and the temperature is equalized across the sample thickness. For instance, in a silicon wafer 0.4 mm thick, the temperature is equalized during the act of illumination provided that the absorption coefficient of silicon is $10^4 - 10^5$ cm^{-1} (Ref. 64) and light is absorbed within a layer $\sim$1 μm thick. According to calculations,[30,65,66] at these durations of irradiation using xenon lamps the temperature difference between the opposite surfaces of the silicon wafer is expected to be of the order of a few degrees.

Problems mainly concern the parameterization of the process. The following parameters should be controlled:

— the radiation energy supplied to the sample and the absorbed radiation dose;

— the temperature of the irradiated sample,[67,68] the lateral temperature distribution;[65,69] and

— thermal kinetics as a generalized parameter suitable for optimization of the process.[70]

These problems become more complicated as the geometry of samples made of the same material changes and moreover on going from one material to another.

By analyzing the optical absorption spectra of some materials it was found which portion of the emission spectrum of a xenon lamp can be efficiently used for activation of processes in a particular system. For instance, light absorption by germanium crystals occurs in almost entire emission range, whereas silicon and $BaTiO_3$ crystals absorb light in the ranges up to 1000 nm and up to 400 nm, respectively. It was also found that quartz, sapphire and LiF crystals utilized as substrates for film growth are completely transparent to light of xenon lamps. Estimation for metals is complicated because of different reflectance spectra. The reflectance spectra of Ag, Al, Au, Cu and Pt films constructed using the data of Ref. 71 for the emission range of a xenon lamp are presented in Fig. 2. As can be seen, each metal requires fine tuning of a particular irradiation regime to ensure activation of the desired processes.

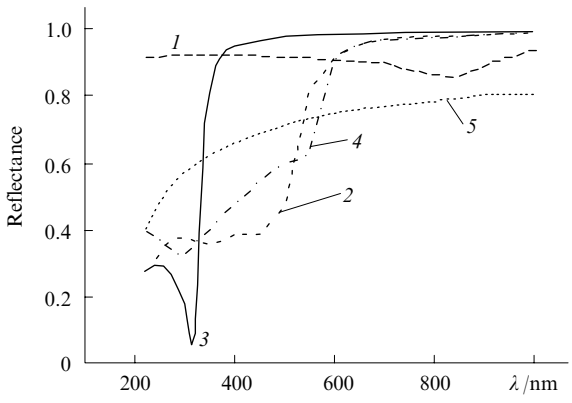


Figure 2. Spectral dependences of the reflectance of aluminium (*1*), gold (*2*), silver (*3*), copper (*4*) and platinum (*5*) films in the emission region of xenon lamps (plotted using data taken from Ref. 71).

To parameterize the photon treatment procedure for any sample, it is appropriate to use the quantity equal to the radiation energy supplied to the sample per unit surface area (E_e); for a particular sample one can evaluate the temperature reachable (T_r) at a given energy. A possible approach to the determination of E_e in a particular setup was reported.[62,72] Radiation from a xenon lamp was received by a 0.4-mm thick copper plate (surface area 4 cm^2) coated on one side with an Al_2O_3/Al composite layer deposited by magnetron sputtering of aluminium in oxygen atmosphere.[73] The temperature of the plate was controlled by a thermocouple and a fast recording device. It was accepted that high open porosity characteristic of this coating[74] ensured almost complete absorption of radiation (a black body equivalent). Therefore, E_e was assumed to be equal to the integral radiation dose absorbed by the plate at different lamp current values and irradiation times, namely, $cm(T_r - T_0)$, where c is the heat capacity, m is the mass of the plate and T_0 is the initial temperature of the plate (Fig. 3 *a*). If the role of a receiver was played by a single-crystalline silicon wafer, the temperatures attained were estimated

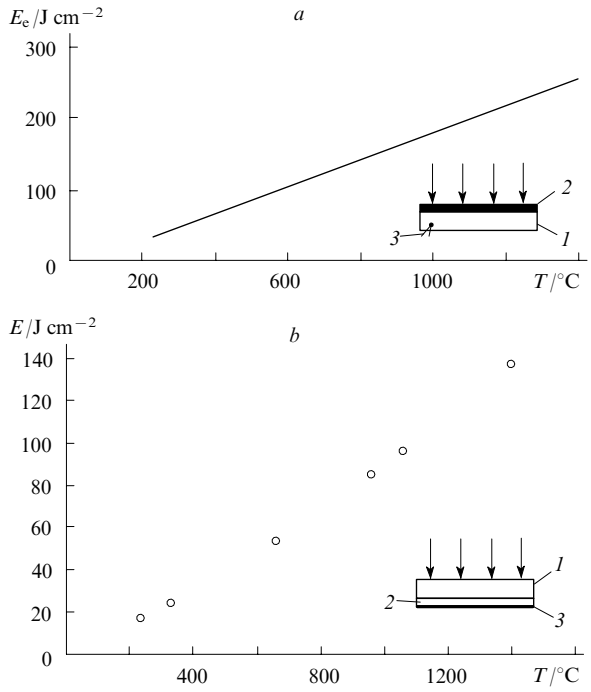


Figure 3. Temperature dependences of the radiation energy supplied to the sample (*a*) and absorbed by the sample (*b*).[62,72] (*a*) Calculations[62,72] using the temperature values in the range 230–1030 °C attained by a black body for a particular setup; copper plate (*1*), a layer of Al_2O_3/Al black composite coating (*2*) and thermocouple (*3*); (*b*) calculations of the energy absorbed by the heterostructure and corresponding to heating to the melting point of the metal (Sn, Pb, Al, Ag, Au) film and the silicon surface; Si wafer (*1*), SiO_2 film (*2*) and metal film (*3*).

from the melting of Sn, Pb, Al, Ag and Au films deposited on the nonirradiated side of the wafer and from the onset of silicon melting. The calculated absorbed radiation energies corresponding to these temperature estimates are presented in Fig. 3 *b*.

The spectrum of the xenon lamp has the most part of power output in the vacuum UV region[25] which plays an important role in the acceleration of activated processes (going from halogen lamps to xenon lamps as sources of radiation made it possible to reduce the treatment duration by two orders of magnitude). Also, in most cases this spectral region is of crucial importance for manifestation of the photon activation effect itself. In this connection, the effect of laser radiation at different wavelengths on the clean surface of copper single crystals is remarkable, *viz.*, only short-wavelength radiation produced defects in the form of nanoscale adatom and vacancy islands.[75] A comparison of the effect of radiation from different sources (in all cases, the spectra included the UV and vacuum UV regions) on silicon revealed[25] that it was the lifetime of minority charge carriers in silicon that increased to the greatest extent as the wavelength decreased.

The results of original studies showed the efficiency of rapid photon treatment in the processes mentioned above; they were reported in numerous publications and generalized in monographs.[30,76,77] In particular, mention was made that practical application of rapid photon treatment is ahead of investigations on the nature of the effect of direct action of photons on processes in inorganic materials.

This review is focused on (i) experimentally observed effect of photon activation *per se*, which manifests itself in solid-phase processes (synthesis of various compounds, crystallization, recrystallization, diffusion) as compared to the classical isothermal annealing and (ii) on the hypotheses concerning the mechanism of athermal contribution of photon treatment to these processes.

II. Synthesis of metal silicide films

Solid-phase synthesis of metal silicides with thermal activation of the reaction between silicon and metal films deposited on its surface has been much studied[78,79] in connection with the design of electrodes, gates, contacts and interconnectors for semiconductor devices.[80] To date, all practically valuable silicides were analyzed within the framework of conventional thermal processing approach and regularities of structural and phase transformations occurring during the reaction, temperature regimes of the formation of the final phases, the structure of phase boundaries in Si/silicide heterosystems with small structural and size mismatch between the crystal lattices (first of all, Si/$NiSi_2$ and Si/$CoSi_2$ systems) were established.

Miniaturization of functional elements used in information system technologies down to submicrometre size made the silicide synthesis regimes involving long-term thermal processing inappropriate. In this connection, the first studies[1–6] on photon treatment of single-crystalline silicon/thin metal film heterostructures demonstrated the efficiency of the procedure in the synthesis of silicide films (Fig. 4). Namely, the duration of silicide formation reduced appreciably, the concentration profile in the region of phase boundary became sharper and the effect of accompanying gases weakened. In particular, the possibility of synthesis of a palladium silicide film in air by illuminating the Pd ($\sim$50 nm)/Si heterostructure with light of a xenon lamp for 1.25 s was demonstrated.[81] The effect of photon treatment manifested itself in the electric properties of the Si/Pd_2Si heterostructure as a decrease in the reverse branch current in the $I-V$ curve.

In the case of photon activation, the grain structure of the silicide is more dispersed than that formed upon conventional thermal processing. This is clearly seen despite the fact that in both cases, chemoepitaxy of Pd_2Si on the Si(111) surface in two equivalent orientations (three orientations for PtSi) leads to the formation of nanocrystalline textures. Equivalence of orientation relationships between the silicide and silicon lattices in each system ensures stability of the textures and grain structure of the silicide on heating to the eutectic temperature.[82]

By varying the duration of photon treatment (and thus the energy supplied to the heterostructure) and the attainable temperature one can reveal intermediate silicide phases in the system under study.[83,84] The cross-sectional TEM images of the samples in the Si(111)/$TiSi_2$ system fabricated at photon treatment durations of 1.4 and 2.0 s are shown in Figs 5 and 6, respectively. Judging from titanium epitaxy (see Fig. 5 *a*), the quality of the chemically etched Si(111) surface was sufficient for the reaction to occur.

The formation of bilayer silicide [the lower epitaxial layer is $TiSi_2$ (C49), the upper one is Ti_5Si_3] takes 1.6 s. In both cases, the near-surface region $\sim$10 nm thick contains a

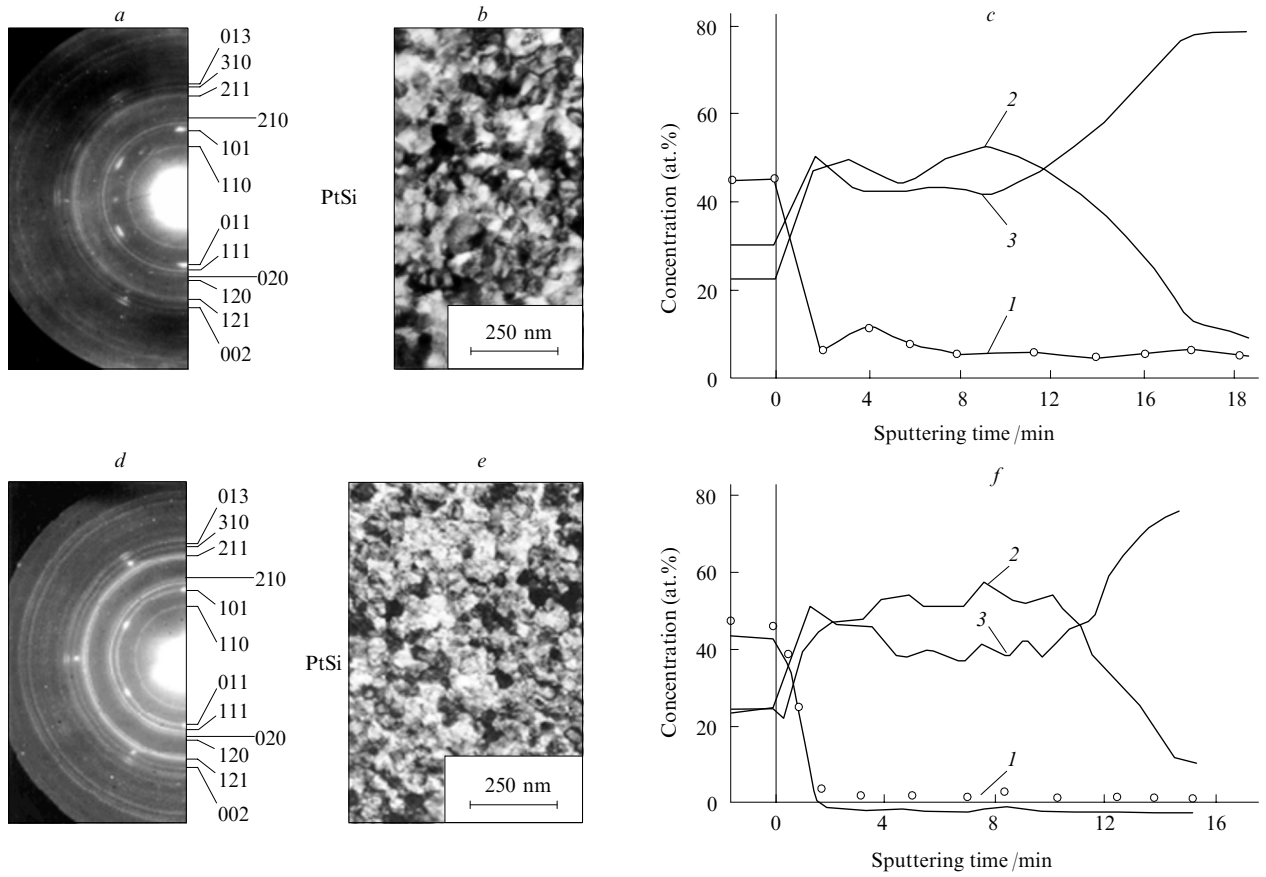


Figure 4. Fragments of electron diffraction patterns (*a*, *d*); TEM images of the structure of PtSi films (*b*, *e*) and the oxygen (*1*), platinum (*2*) and silicon (*3*) concentration profiles with film thickness (*c*, *f*).[5]
Synthesis in H_2 atmosphere followed by thermal processing at about 780 K for 30 min (*a*–*c*); photon treatment in air for 1.25 s (*d*–*f*).

mixture of titania and titanium carbide. After 2.0 s, the formation of single-phase silicide $TiSi_2$ (C54) is almost completed (see Fig. 6 *b*). This is confirmed by the concentration-with-thickness profiles of the elements constituting the heterostructure (Fig. 7) and by the Auger spectrum of the surface layer (see Fig. 6 *a*); the latter also indicates excess concentrations of carbon and oxygen atoms in this layer. In the bulk of the film, the silicide is enriched with silicon (see Fig. 7 *a*). This characterizes the main role of diffusion of silicon atoms and confirms the well-know idea

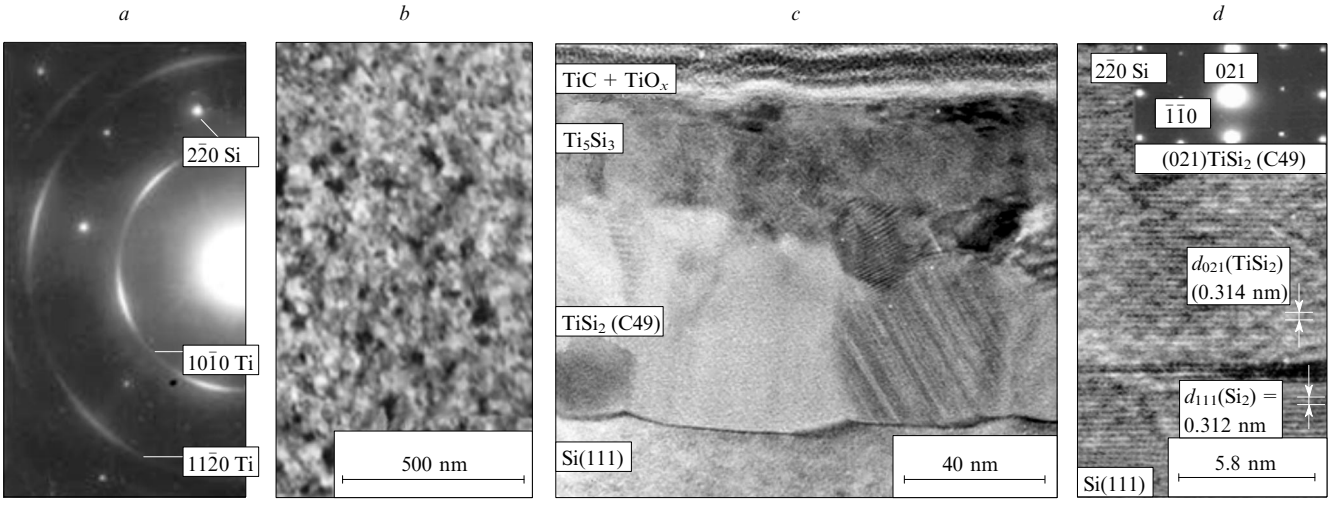


Figure 5. Fragment of an electron diffraction pattern (*a*) and TEM image (*b*) of the initial heterostructure Si(111)/Ti (40 nm); cross-sectional TEM images of the sample after photon treatment for 1.6 s (*c*, *d*).[83,84]

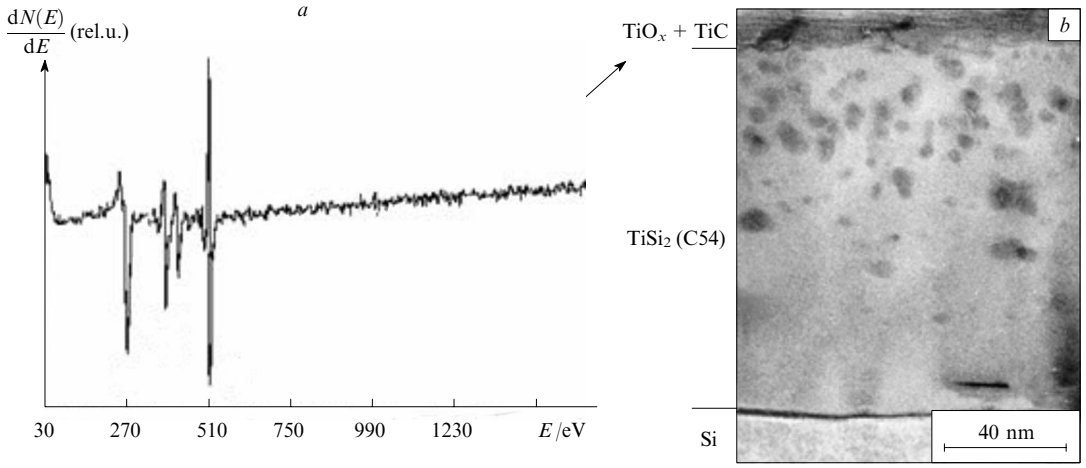


Figure 6. Auger electron spectrum of the surface layer (*a*) and cross-sectional TEM image of the sample of Si(111)/Ti heterostructure after photon treatment for 2 s (*b*).[83, 84] $N(E)$ is the number of Auger electrons.

that the mechanism of formation of refractory metal silicides is based on silicon diffusion throughout the metal and the silicide formed.[78, 79]

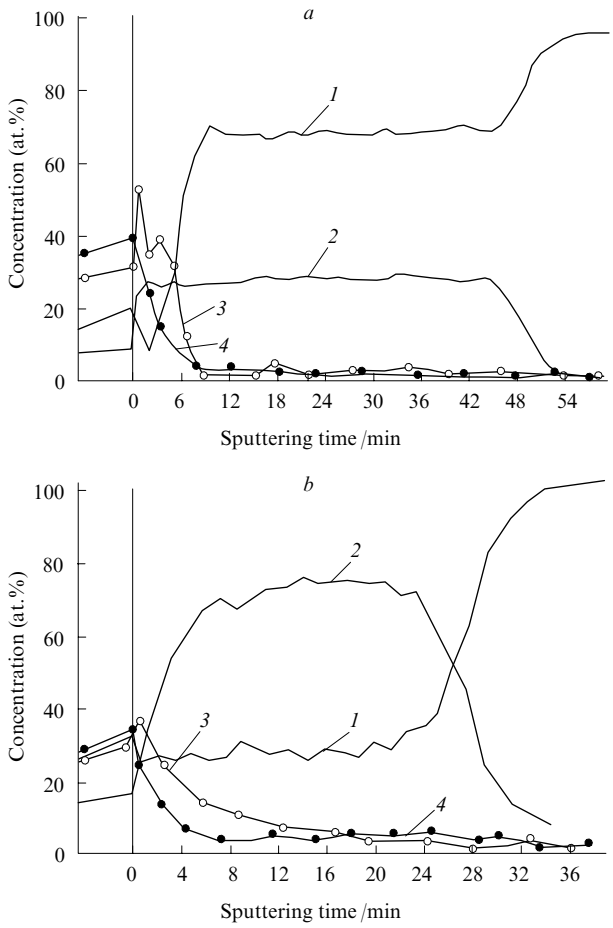


Figure 7. Concentration profiles of silicon (*1*), titanium (*2*), oxygen (*3*) and carbon (*4*) with thickness of the Si(100)/Ti heterostructure.[83, 84]
Photon treatment duration /s: 2 (*a*) and 1.4 (*b*).

The dependence of the resistance (R_s) on the duration of photon treatment (Fig. 8) allows one to reveal steps corresponding to the saturation of titanium film with silicon atoms (ascending branch of the plot), to the starting point of the reaction and to the reaction completion (minimal resistance of the silicide film). Interestingly, under conditions of short-term irradiation (*e.g.*, 1.4 s), the film is saturated with silicon atoms to a concentration of about 20 at.% (according to the equilibrium diagram of state, the solubility of silicon in titanium is at most 2 at.%!) but no nucleation of silicide phases is detected. Probably, the nanocrystalline structure of the initial titanium film (average nanograin size is a few nanometres) favours fast grain boundary diffusion of silicon atoms and their segregation at grain boundaries. An increase in the photon treatment energy activates fast reaction of silicide formation because the reaction front is distributed over the entire volume of the film (starting from the silicon-saturated nanograin boundaries). At high radiation energies, silicon atoms go to the surface of the metal, and the silicide may be coated with silica.[85]

The effect of flash annealing on the phase transformations, orientation and substructure transformations occur-

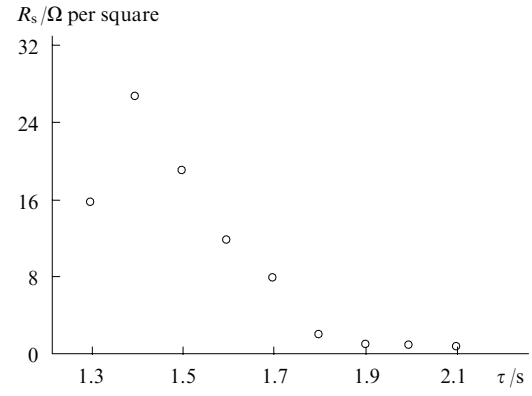


Figure 8. Surface electrical resistance of Si(111)/Ti heterostructure plotted *vs.* photon treatment duration.[83]

ring in the heterostructure Si(111)/Ni (film)/Pt (film) was studied.[86] The starting heterostructures Pt (25 nm)/Ni (20 nm)/Si(111) (380 μm)/Ni (20 nm)/Pt (25 nm) were produced by ion plasma sputtering and successive condensation of metals on both surfaces of a silicon wafer. Illumination with light of xenon lamps was carried out in vacuum (10^{-3} Pa), the energy density at the surface of the sample was in the range 185–285 J cm^{-2} and the irradiation time was 1.3–2 s. The wafer was irradiated from one side, the temperature was assumed to be uniform across the sample,[30, 65, 66] so the back (nonirradiated) side of the wafer was in the rapid thermal annealing conditions.

The results of investigation of the phase composition and structure of the silicides formed on both sides of the wafer were compared with the results of 30-min isothermal annealing of the initial heterostructures in vacuum (10^{-3} Pa) at 350, 400, 500, 600, 700 and 800 °C.

At E_e = 185 J cm^{-2}, a metal-enriched silicide $(Pt,Ni)_2Si$ with an orthorhombic structure similar to that of Pd_2Si ($P6_2m$) and the silicides $Pt_{1-x}Ni_xSi$ and $Ni_{1-y}Pt_ySi$ are formed on the irradiated side (photon treatment regime). The surface layer of the silicide heterostructure also contains a fine-grained, porous solid solution Pt—Ni. The lattice parameters of the silicides are listed in Table 1. The silicide heterostructure represents a layered system $Si(111)/Ni_{1-y}Pt_ySi/Pt_{1-x}Ni_xSi/(Pt,Ni)_2Si$. The phases have a biaxial texture and consist of nanocrystalline grains up to 40 nm in size (Fig. 9). For the same lattice symmetry of the solid-solution silicides, the orientation relationships can be written as follows:

$$(010), [100]Pt_{1-x}Ni_xSi, Ni_{1-y}Pt_ySi, (Pt,Ni)_2Si \parallel \quad (1)$$

(111), [112], [121] and [211] Si

Only single-phase silicide (Pt, Ni)$_2$Si with an average grain size of nearly ~20 nm is formed on the nonirradiated side (*i.e.*, under rapid thermal annealing conditions).

At E_e = 230 J cm^{-2}, the silicide film on the irradiated silicon surface is characterized by a bimodal size distribution of $Pt_{1-x}Ni_xSi$ grains, namely, large crystallites (~500 nm in size) are surrounded by fine matrix grains (up to 50 nm in size) according to relationship (1). This substructure of the film, accompanied by changes in texture, results from secondary recrystallization.[87]

At E_e = 245 J cm^{-2}, a homogeneous polycrystalline layer of the silicide $Pt_{1-x}Ni_xSi$ with grains to 2 μm in size is formed on both sides of the silicon wafer. The average grain size is about 800 nm on the irradiated side and 500 nm on the back side.

At E_e = 285 J cm^{-2}, the silicide film crystallizes from melt on both sides of the silicon wafer. This indicates identical thermal conditions on the two sides of the wafer.

A comparison of the phase compositions and substructures of the silicides formed on both sides of the wafer at different E_e values showed that the effect of photon treatment manifests itself in faster solid-phase reaction of silicide formation in the irradiated heterostructure. At E_e = 185 J cm^{-2}, the lower silicide $(Pt,Ni)_2Si$ is also formed, but illumination activates the formation of higher phases based on solid solutions as well.

Under isothermal annealing conditions, diffusion in the system proceeds more slowly. At 350 °C, the nickel layer is the first to react with the substrate to give hexagonal Ni_2Si ($P63/mmc$). The heterostructure thus formed is Pt/(Pt,Ni)/Ni_2Si/Si(111). Owing to the small mismatch between the lattice parameters in the basal plane, the silicide Ni_2Si grows epitaxially in the orientation relationship

$$(0001)[1120]Ni_2Si \parallel (111)[110]Si \quad (2)$$

At 400 °C, the heterostructure Pt/(Pt,Ni)/Ni_2Si/$Pt_{1-x}Ni_xSi$/Si(111) is formed. The grain size of the platinum film remains essentially unchanged.

At 500 and 600 °C (E_e = 215 and 230 J cm^{-2}, respectively), one deals with the formation of bilayer silicide heterostructures similar to those produced under the rapid thermal annealing conditions. Unlike the photon treatment, isothermal annealing leads to simultaneous formation of two polymorphs of the silicide $Ni_{1-y}Pt_ySi$, *viz.*, the (main) hexagonal phase (judging from the spot intensities in the electron diffraction pattern) in the orientation relationship

$$(0001)[1120]Ni_{1-y}Pt_ySi \parallel (111)[110]Si \quad (3)$$

Table 1. Phase compositions of thin films of solid-solution silicides formed uner different photon treatment and thermal processing regimes.[86]

Photon treatment									Thermal processing				
E_e /J cm^{-2}	phases on the irradiated side of the wafer	lattice parameters /nm			phase on the back side of the wafer	lattice parameters /nm			T/°C	phases	lattice parameters /nm		
		a	*b*	*c*		*a*	*b*	*c*			*a*	*b*	*c*
185	$Ni_{1-y}Pt_ySi$	0.569	0.520	0.335	$(Pt,Ni)_2Si$	0.598	0.560	0.344	350	Ni_2Si(H)	0.3805	—	0.489
	$Pt_{1-x}Ni_xSi$	0.588	0.547	0.350									
	$(Pt,Ni)_2Si$	0.598	0.560	0.344									
215	$Ni_{1-y}Pt_ySi$	0.569	0.520	0.330	$Ni_{1-y}Pt_ySi$	0.569	0.520	0.330	500	$Ni_{1-y}Pt_ySi$(H)	0.328	—	0.522
										$Ni_{1-y}Pt_ySi$(R)	0.569	0.520	0.330
	$Pt_{1-x}Ni_xSi$	0.586	0.544	0.348	$Pt_{1-x}Ni_xSi$	0.586	0.544	0.348		$Pt_{1-x}Ni_xSi$	0.586	0.544	0.348
230	$Pt_{1-x}Ni_xSi$ (see [a])	0.578	0.540	0.344	$Ni_{1-y}Pt_ySi$	0.569	0.520	0.330	700	$Pt_{1-x}Ni_xSi$ (see [a])	0.578	0.540	0.344
					$Pt_{1-x}Ni_xSi$	0.584	0.542	0.347					
245	$Pt_{1-x}Ni_xSi$ (see [a])	0.574	0.536	0.342	$Pt_{1-x}Ni_xSi$	0.574	0.536	0.342	800	$Pt_{1-x}Ni_xSi$ (see [a])	0.574	0.536	0.342

[a] Coarse-grain silicide.

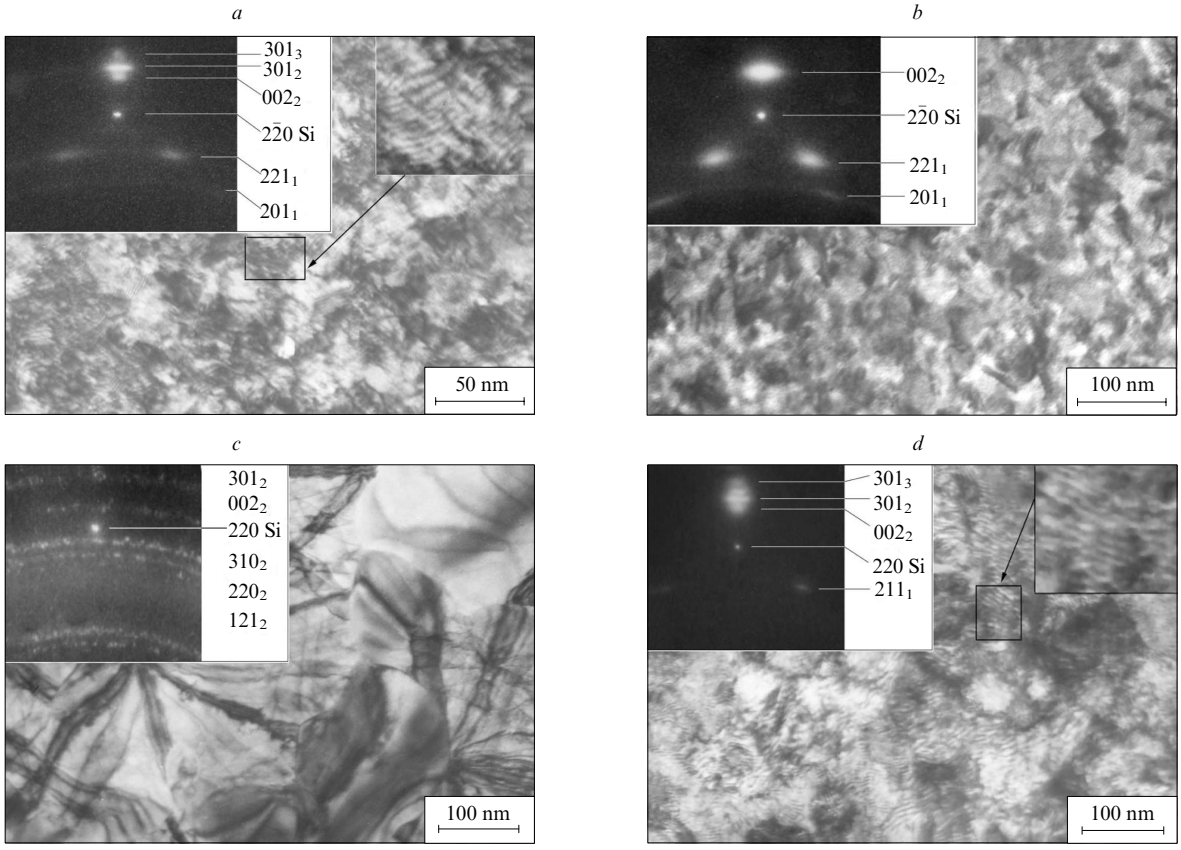


Figure 9. TEM images and fragments of electron diffraction patterns characterizing the structure and phase compositions of silicides formed upon irradiation of one side of the Pt/Ni/Si(111)/Ni/Pt heterostructure.[86]
Irradiated side (*a*, *c*), back side (*b*, *d*); E_e/J cm^{-2}: 185 (*a*, *b*) and 230 (*c*, *d*); the subscripts 1, 2 and 3 denote the silicide phases $(Pt,Ni)_2Si$, $Pt_{1-x}Ni_xSi$ and $Ni_{1-y}Pt_ySi$, respectively.

and the orthorhombic phase in the orientation relationship (1). The formation of the hexagonal phase is consistent with the published data.[88]

As the temperature increases, the parameters of $Pt_{1-x}Ni_xSi$ approach those of NiSi due to the increase in the nickel content. At 700 and 800 °C, single-phase silicide $Pt_{1-x}Ni_xSi$ is formed. At 700 °C, the film consists of randomly oriented individual crystallites (up to 300 nm in size) in the same silicide matrix comprising smaller grains (up to 100 nm in size) in the orientation relationship (1).

A comparison with analogous results obtained under photon treatment (E_e = 245 J cm^{-2}, nonirradiated side) revealed the development of accumulative recrystallization of fine-grained oriented silicide upon long-term annealing at 700 °C, whereas secondary recrystallization is less efficient. At 800 °C, a film of silicide $Pt_{1-x}Ni_xSi$ with randomly oriented crystallites up to 2 μm in size is formed. The film is similar to that produced under pulsed photon treatment at E_e = 245 J cm^{-2}.

By comparing the threshold values of the energy E_e and the temperatures of formation of the same phases (see Table 1) one can evaluate the effect of photon activation:

— formation of metal-enriched silicide $(Pt,Ni)_2Si$ in the course of photon treatment at E_e = 185 J cm^{-2} (process duration is 1.3 s) and Ni_2Si in the course of thermal processing at 350 °C for 30 min indicates a higher diffusion activity of components in the former case;

— the formation of only orthorhombic silicide $Ni_{1-y}Pt_ySi$ upon photon treatment *vs.* simultaneous formation of the hexagonal (major phase) and orthorhombic phases upon thermal processing;

— reduction of the temperature of formation of the corresponding silicide phases by 100–150 °C compared to conventional thermal processing.

Taking into account the fact that the formation of silicides is diffusion-controlled, acceleration of the process upon photon treatment can also be explained by photostimulated formation of nonequilibrium vacancies in the metal film[89–91] and weakening of atom–atom bonds in silicon. The observed acceleration of gold diffusion in silicon upon photon treatment[22] was explained[92,93] using the idea of multiply excited sites (g^i is the proportion of such sites, i is the multiplicity of excitation) or sites with two singly-excited bonds in silicon. Estimation showed that at a power density of about ~300 W cm^{-2}, the proportions of singly and doubly excited sites in the near-surface layer are $g^1 \approx 10^{-3}$ and $g^2 \approx 10^{-6}$, respectively. Assuming that the activation barrier to generation of Frenkel pairs (ΔE) decreases in proportion to the multiplicity of excitation (ΔE = 1.0–1.2 eV for i = 2), fast metal diffusion across the multiply excited sites becomes possible. The preferred direction of diffusion during the synthesis of metal silicides depends on a particular system (*e.g.*, diffusion of nickel in silicon, diffusion of silicon in titanium).

Assuming that the intensity of radiation supplied to the silicon crystal in the 'thin metal film/single-crystalline silicon wafer' heterosystem is almost two orders of magnitude lower than that supplied to the surface of the heterostructure, the proportion of doubly excited bonds in the near-surface layer will correspondingly decrease. As to the condensed metal film (*e.g.*, a Ti film), its nanocrystalline structure itself provides a channel of rapid grain-boundary diffusion of silicon atoms and the effective intra-grain diffusion distance is only limited by the nanograin size. At the same time, it was shown that under laser irradiation of metal films the concentration of nonequilibrium vacancies responsible for the increase in the grain growth rate (photostimulated recrystallization) can increase to a value of 10^{-4} (Refs 89–91).

Possible mechanisms of photon activation of processes controlling the synthesis of silicides were studied.[83] Taking the synthesis of single-phase up to 150 nm thick silicide $TiSi_2$ as an example, the absorbed power density calculated with allowance for reflectance from the metal film is about 30 W cm^{-2} and corresponds to the photon flux

$$N_q = 30/33 \times 10^{-20} \approx 10^{20}\ s^{-1}\ cm^{-2}$$

(33×10^{-20} is the power density per photon).

The energy of photons (from 1 to 6 eV) is sufficient to activate the formation and diffusion of vacancies in silicon (2.1–2.3 and 1.1 eV, respectively).[94] For a titanium film (absorption coefficient $\mu_{Ti} = 2.5 \times 10^{-7}\ m^{-1}$) with the thickness $h = 6 \times 10^{-8}$ m, the intensity of light incident on the silicon surface is

$$I = I_0 \exp(-\mu h) \approx 0.21$$

Assuming the light absorption coefficient of silicon $\mu_{Si} = 5 \times 10^4\ cm^{-1}$, for a film 0.01 mm thick one gets

$$\Delta I_{ab} \approx 10^{-4} I_0$$

i.e., the absorbed photon flux is

$$\Delta N_q \approx 10^{20} \times 10^{-4} \approx 10^{16}\ s^{-1}\ cm^{-2}$$

Absorbed photons excite the same number of atoms. The average lifetime of an excited atom is $\sim 10^{-7}$ s. Assuming that the Frenkel vacancy pair is formed with a 100% probability during the excited-state lifetime, the vacancy lifetime is about 1 s; if the number of atoms in the same layer is 5×10^{19}, the concentration of vacancies is nearly 10^{-4}; this is sufficient for abnormally fast diffusion to occur. Despite the fact that this approach and the calculation procedure provide only a partial explanation for the effect observed (namely, the parameter values are overestimated), acceleration of diffusion due to creation of nonequilibrium vacancy concentration in the metal film and in the semiconductor under photon treatment conditions seemingly does occur.

Diffusion can be activated by the action of 'hot' electrons injected from the metal film to the semiconductor and responsible for abnormal decrease in the activation energy of atomic diffusion and weakening of atom–atom interactions. Owing to absorption of photons, electron gas in the metal film goes to the excited state (the surface concentration of free electrons is about 10^{17} cm^{-2} for a 60-nm thick film). Assuming that electron–phonon interaction causes conversion of the energy of photons to the energy of phonons (E_{ph}) without loss, illumination of 1 cm^2 over a period of 1 s may create an additional number of phonons (N'_{ph})

$$N'_{ph} = N_q \frac{\langle \hbar\omega \rangle}{E_{ph}} = N_q \frac{\langle \hbar\omega \rangle}{KT} \approx 10^{20} \frac{2.5}{0.005} \approx 5 \times 10^{22}$$

which is comparable with the proper number of phonons in the same volume

$$N_{ph} = \frac{9}{2} \left(\frac{N_A}{V}\right) \left(\frac{T}{\theta}\right) \approx 10^{22}$$

Here ω is the frequency, θ is the Debye temperature, N_A is the Avogadro constant and V is the molar volume.

Owing to long mean free path of phonons in metal and silicon and to high velocity of sound, phonons are almost immediately uniformly distributed in the bulk of the heterostructure, which causes a uniform increase in temperature. Even assuming that the mean free path of phonons in the metal/semiconductor transient layer equals the interatomic distance, the excess concentration of phonons in the metal film for a given temperature is a few hundredths of a per cent. Therefore, the pure photon effect of pulsed photon treatment is too weak to be responsible for the accelerated growth of silicides.

The following mechanism was also considered.[83] Electrons in metals have a mean free path of about 10^{-5} cm. To dissipate the excess energy, nonequilibrium excited electrons should execute ~ 1000 collisions with phonons, *i.e.*, to travel a distance of 10^{-2} cm. This means that almost all electrons in the metal film can reach the surface of the semiconductor without loss of the excess energy. The number of electrons transferred to the semiconductor is determined from thermodynamic considerations.

The Fermi level difference between the metal and the semiconductor is responsible for electron transfer from the conductor to the semiconductor which proceeds until equalization of both Fermi levels. Equalization is accompanied by the appearance of a contact potential difference ($\Delta\varphi$) between the semiconductor and the metal. The average strength of the contact field is given by

$$E_c = \frac{\Delta\varphi}{ed} = \frac{3}{1.6 \times 10^{-19} \times 2.5 \times 10^{-10}} = 1.2 \times 10^{10}\ V\ m^{-1}$$

Here e is the electron charge and $d \approx 2.5 \times 10^{-10}$ m is the distance (v) between metal and semiconductor.

Considering the electric field at the metal/semiconductor interface as electric field in a flat capacitor and following the Gauss theory, the charge density on the capacitor plates is

$$\sigma_s = \varepsilon_0 E_c$$

and the number of electrons necessary to create such a charge density is

$$n = \frac{\sigma_s}{e} = \frac{\varepsilon_0 E_c}{e} \approx 6 \times 10^{13}\ cm^{-2}$$

Injected electrons with an excess energy of about 3 eV (n) increase the chemical potential of the near-interface layer of the conductor containing N_{at} atoms by

$$\frac{\Delta\varphi n}{N_{at}} \approx \frac{2 \times 10^{14}}{2 \times 10^{15}} \approx 10^{-1} \text{ eV}$$

which corresponds to an increase in the effective temperature of the conductor by nearly 1000 K. The excited electron subsystem of the semiconductor supersaturated with carriers causes deformation of the potential relief for atoms in the near-boundary layer; this may probably involve the hybridization of chemical bonds. This is equivalent to multiple excitation of atom–atom bonds and ensures fast diffusion and interaction.

A strong dependence of diffusion of gold atoms on the type of silicon doping under photon treatment conditions was found.[22] Namely, diffusion in n-Si proceeds better than in p-Si; therefore, the concentration of gold in the former case is nearly two orders of magnitude higher than in the latter case. This dependence can be explained by partial capture of injected electrons by acceptor impurities.

Apparently, one should expect a strong dependence of the effect of photon treatment on the spectral composition of the photon flux. A decrease in the average energy of photons $\langle\hbar\omega\rangle$ will cause a decrease in the number of injected electrons and their excess energy $\Delta\varphi$, *i.e.*, the effect of photon treatment is proportional to $\langle\hbar\omega\rangle^2$. This is confirmed by numerous experimental data on activation of some processes by irradiation with light of halogen and xenon lamps, namely, the necessary duration of illumination with light of halogen lamps is two orders of magnitude longer than in the case of xenon lamps.

III. Recrystallization of thin films

Thermal processing of thin, highly disperse polycrystalline films with random orientations (*e.g.*, films condensed on non-orienting unheated substrates) causes both primary and accumulative recrystallization[87] due to migration of grain boundaries. These processes lead to multiple increase in the grain size owing to 'coalescence' of grains driven by minimization of the interface energy.

Accumulative recrystallization of thin films of fcc metals can be stimulated by pulsed laser irradiation at 1.06 μm.[95–97] Compared to continuous thermal processing, the effect manifested itself as two- or threefold increase in the grain size and grain growth rate. This was explained by generation of nonequilibrium vacancies whose concentration increased by more than two orders of magnitude when the film was rapidly heated by short pulses. Also, no film break into islands was observed under rapid laser treatment. This is of paramount importance for, *e.g.*, photon activation of diffusion of gold atoms in silicon in order to compensate for minority charge carriers.[98] Thermal processing causes disintegration of a film on the clean surface of single-crystalline silicon wafer; this is favoured by heating to the eutectic temperature. Under photon treatment, the film continuity and, correspondingly, the entire diffusion front is retained. Solid-phase epitaxy of gold in the optimal orientation relationship (Fig. 10)

$$(110),[001]\text{Au} \parallel (001), \langle 110\rangle\text{Si}$$

indicates a good Si(001)/Au phase boundary.

The influence of illumination with light of a xenon lamp on recrystallization of 50-nm Pt, Pd and Au thin films was studied.[99] Heterostructures M/SiO_2/single-crystalline silicon wafer/SiO_2/M were fabricated by depositing metal films on both sides of an oxidized silicon wafer 340 μm thick. Irradiation of the heterostructure on one side only enables realization of the rapid photon treatment regime on the irradiated side and rapid heat treatment regime on the back side (owing to radiation absorption in the near-surface layer on the irradiated side). This occurs in identical thermal conditions taking into account the small difference between the temperatures attained on irradiation on both sides of the heterostructure (see above).

The TEM images of structures with thin gold film presented in Fig. 11 illustrate the effect of photon activation. The initial structures are nanodispersed; in particular, the average gold grain size is about 20 nm. Although the grain structure of the films in all steps of annealing for all

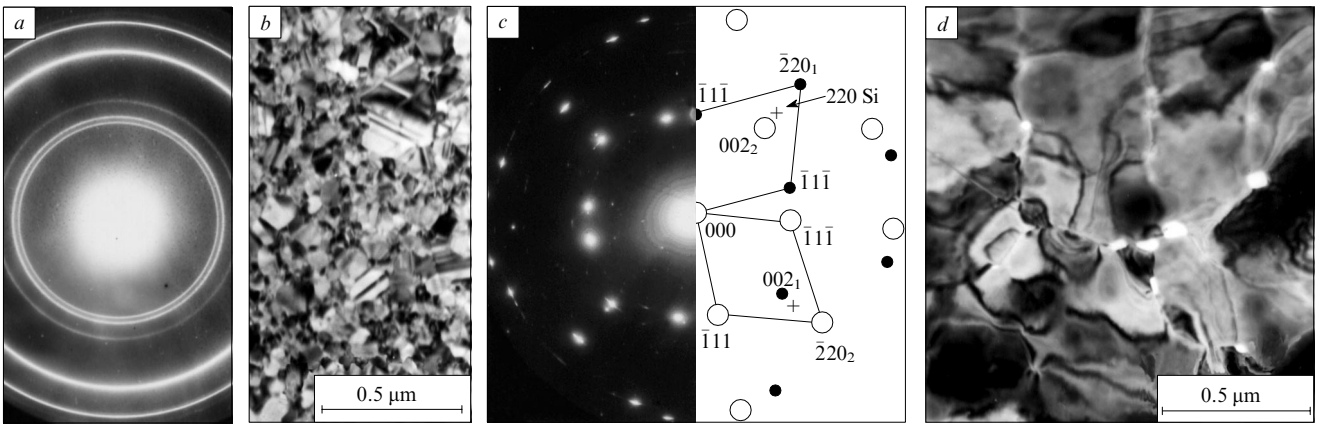


Figure 10. Electron diffraction patterns (*a*, *c*) and TEM images (*b*, *d*) illustrating structural and orientational transformations upon photon treatment of a gold film on Si(001) surface.[98]
Initial structure (*a*, *b*) and irradiated structure (*c*, *d*).

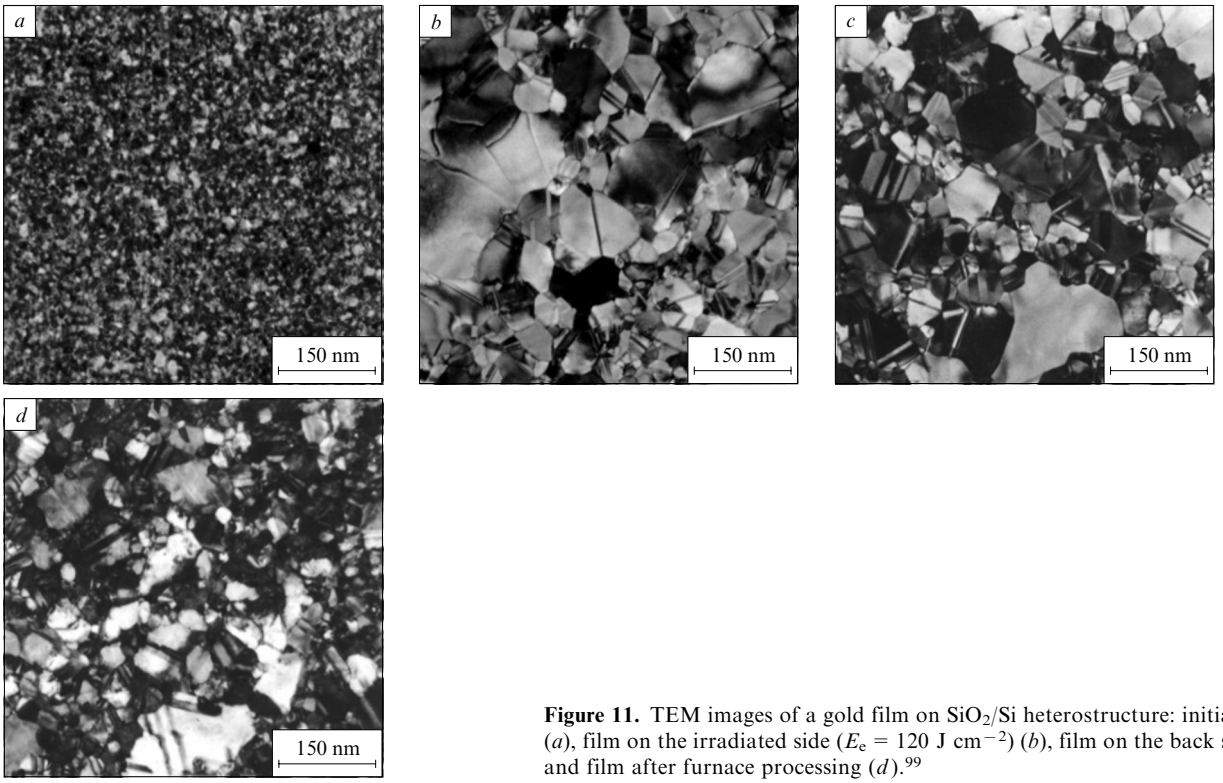


Figure 11. TEM images of a gold film on SiO_2/Si heterostructure: initial state (*a*), film on the irradiated side (E_e = 120 J cm^{-2}) (*b*), film on the back side (*c*) and film after furnace processing (*d*).[99]

samples studied is highly inhomogeneous, the average grain sizes after photon treatment and after the corresponding thermal processing are clearly different, which indicates a higher grain growth rate in the former case. Certain microscopic regions recrystallize at different rates; an increase in E_e upon photon treatment and an increase in temperature upon thermal processing causes a relative increase in the size of coarse-grain domains and a decrease in the size of small-grain regions.

A comparison of the grain structure of gold films upon rapid photon treatment (see Fig. 11 *c*) and furnace processing (see Fig. 11 *d*) revealed an identical character of structural transformations. In particular, photon treatment of gold films with heating to temperatures close to the melting point (power density supplied to the sample is E_e = 175 J cm^{-2}; the corresponding temperature of the film is 1340 K) produced changes in the surface relief which became characteristic of the onset of melting of the metal film, which confirms the correctness of estimation of the attainable temperatures.

Quantitative estimates were obtained by calculating the temperature dependences of the average grain growth rate (v) of the metal films under photon treatment and thermal processing conditions. The ln v-*vs*.-$1/T$ plots (Fig. 12) for the equivalent attainable temperatures (T_u) on the back side of the wafer can be approximated, within the limits of measurement error, by straight lines. As can be seen, for all metals in question photon treatment causes a greater increase in the grain growth rate compared to thermal processing. The calculated activation energies for the thermal processing regime are consistent with the known values for the processes controlling migration of grain boundaries.[100]

Much lower activation energies obtained under photon treatment conditions suggest more complicated mechanisms of elementary recrystallization processes compared to the case of thermal processing. In noble metals, electrons absorb the energy of photons in the visible and UV regions; therefore, irradiation of samples with light of xenon lamps causes excitation of electronic subsystems. Most excited electrons undergo nonradiative relaxation.[101, 102] Nonradia-

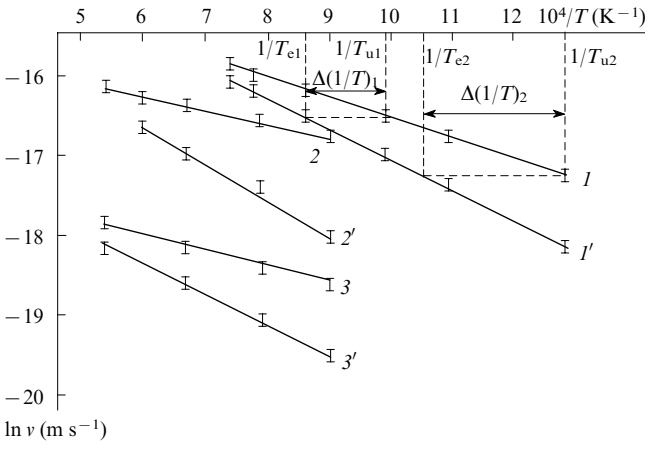


Figure 12. Recrystallization rate plotted *vs*. temperature for gold (*1* and *1′*), platinum (*2* and *2′*) and palladium (*3* and *3′*) films.[99] Photon treatment (*1*–*3*) and thermal processing (*1′*–*3′*). Shown are the $1/T_e$ and $1/T_u$ values characteristic of gold films exposed to photon fluxes with an energy density of 120 J cm^{-2} (T_{e1} = 1170 K, T_{u1} = 1015 K, ΔT_1 = 155 K) and 80 J cm^{-2} (T_{e2} = 955 K, T_{u2} = 775 K, ΔT_2 = 180 K).
Grain growth activation energy /eV: 0.42 (*1*), 0.73 (*1′*), 0.26 (*2*), 0.78 (*2′*), 0.2 (*3*) and 0.58 (*3′*); T_e is the effective temperature characterizing the effect of photon treatment on the irradiated side.

tive decay of an electronic excitation confined within a small volume (point defects, impurities, *etc.*) is due to electron–phonon interaction. If this interaction is rather weak, the localized electronic excitation can be treated as quasi-stationary one, involved in resonant interaction with phonons.[103] Within the framework of the non-stationary perturbation theory, the decay probability of an electronic excitation of some impurity centre depends on the density of the energy states in the vicinity of the quasi-stationary state. Since the number of such states is limited, the decay of an excited electronic state is followed by excitation of only certain normal vibrational modes that are in resonance with the initial state, *i.e.*, only some rather than all normal vibrations of the crystal are excited in the initial step.

Thus, initially, the energy of electronic excitation does not convert to thermal vibrations characterized by uniform energy distribution over all degrees of freedom. Also, a limited number of excited vibrational modes corresponds to atomic vibrations in the crystal whose amplitudes are much larger than those of thermal vibrations. This is equivalent to emission of a large number of phonons from the site where the initial electronic excitation is confined or, in other words, to hypersound of relatively high intensity.

Propagation of hypersonic waves throughout the crystal makes structural rearrangements and formation of point defects more probable. Under conventional thermal processing conditions, this becomes possible owing to a higher temperature. The effect can be described by introducing the effective temperature T_e corresponding to the same vibrational amplitudes. The effective temperature is higher than the attainable (measured) temperature T, but the difference

$$\Delta T = T_e - T$$

decreases as the energy supplied to the sample increases.

When a hypersonic wave propagates throughout the crystal, efficient dissipation of the nonequilibrium state can be attained through the formation of point defects (vacancies and interstitial atoms), which can self-organize and form islands, *i.e.*, irradiation may lead to structural rearrangements in nanoscale regions. Atomic groups (crowdions) formed in the crystal have a low activation energy of migration, namely, a few tenths of an electron-volt per atom (*cf.*, 0.42, 0.26 and 0.2 eV for the activation energy of grain growth in the gold, platinum and palladium film, respectively, under photon treatment conditions). Thus, photon treatment can cause acceleration of self-diffusion (which controls the migration of grain boundaries) due to high mobility of defects, resulting in a decrease in the activation energy of recrystallization.

The nature and mechanism of long-range action of perturbations (illumination, ionization, mechanical action) manifested in changes in the hardness of the metal foil on the back side was explained[104] using the idea of light-induced hypersonic waves.[105–107] In this case, if the foil surface is covered with an oxide layer, the source of the hypersonic wave is associated with internal photoelectric effect. The role of hypersound transmission lines can be played by dislocations.[108]

IV. Nanocrystallization of amorphous structures

Application of photon treatment to activate crystallization was first of all due to the need to recover the structure of the near-surface layers in the semiconductor crystal, which were amorphized upon ion implantation of dopants.[14–18] A microscopic mechanism of stimulated epitaxial crystallization based on the original idea of antibonding quasiparticles that facilitate atomic diffusion was proposed.[109]

Annealing of metal amorphous alloys provides a route to the most compact nanocrystalline structures of corresponding compositions. Photon treatment appeared to be efficient in processing a Fe-based amorphous alloy foil[56–58] and led to its strengthening and improved the magnetic properties.[110] This also holds for nanocrystallization of an Al-based amorphous alloy foil.[111] The appropriateness of such a kind of treatment was substantiated by expectation of a kinetic effect upon rapid energy supply, namely, acceleration of nucleation of the crystalline phases and, correspondngly, higher degree of dispersion of these phases. It was shown that by shortening of the treatment duration to a few fractions of a second one can detect some initial crystallization steps where amorphous alloys still remain ductile.

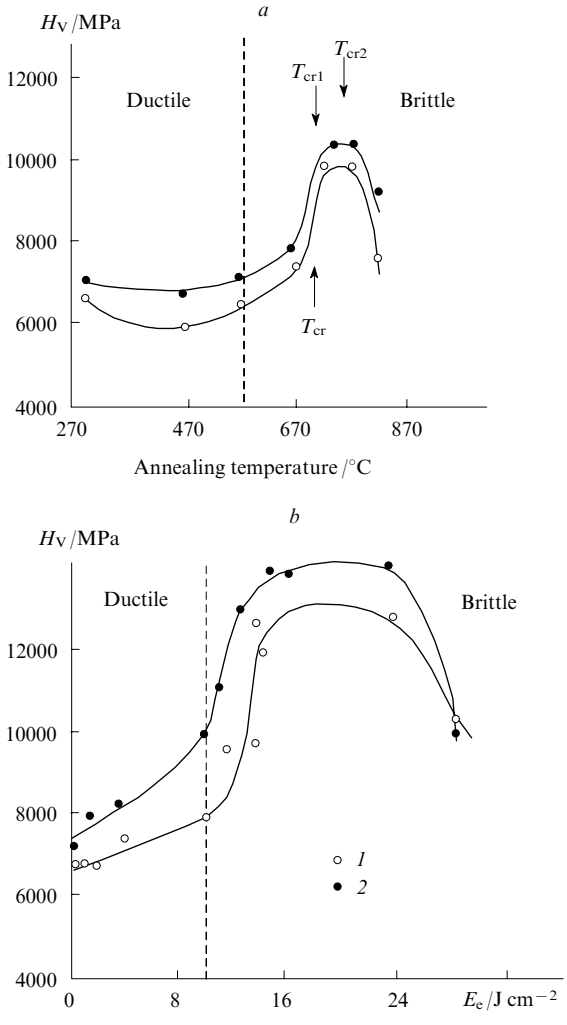


Figure 13. Microhardness of amorphous alloys plotted *vs.* annealing temperature for conventional thermal processing (*a*) and power density under pulsed photon treatment (*b*).[57]
$Fe_{79.3}P_{18.2}V_{2.5}$ (*1*) and $Fe_{76.3}P_{18.2}V_5$ (*2*).

The effect of photon activation of crystallization was illustrated taking foils of amorphous alloys $Fe_{79.3}P_{18.2}V_{2.5}$, $Fe_{76.8}P_{18.2}V_5$ (Ref. 57) and $Fe_{80.5}P_{18.4}Nb_{1.1}$ (Ref. 58) as examples. These alloys were for the first time prepared by the authors of Ref. 112. Amorphization of alloys in the Fe–P–V system was attained by rapid quenching at cooling rates in the range 10^5–10^6 K s^{-1}.

The results of the microhardness (H_V) measurements of amorphous alloys in this system are plotted in Fig. 13 as functions of the annealing temperature (τ = 10 min) and power density (treatment duration varied from 1.0 to 2.8 s).

For both the thermally processed and photon-treated samples, the H_V plots pass through a maximum at temperatures close to the crystallization temperatures (T_{cr}) of the alloys. Photon treatment with 10 J cm^{-2} leads to greater strengthening of the amorphous alloys (by a factor of 1.3) with retention of ductility. An X-ray diffraction study showed that at this power density, the alloys are still amorphous and reveal the formation of nanoscale phases α-Fe, $(Fe,V)_2P$ and σ-phase. The metastable phase $(Fe,V)_2P$ is stable in the second amorphous alloy throughout the entire range of E_e values. According to DTA data (Fig. 14), the amorphous alloy $Fe_{79.3}P_{18.2}V_{2.5}$ crystallizes in a narrow temperature range at 705 K, whereas $Fe_{76.8}P_{18.2}V_5$ exhibits two-step crystallization at T_{cr1} = 725 K and T_{cr2} = 749 K. These data agree with the temperature dependence of resistance.

A comparison of the results of microhardness measurements (see Fig. 13), DTA data and the temperature dependence of resistance (see Fig. 14) showed that the crystallization temperature corresponds to the E_e values in the range 16–20 J cm^{-2}. Interestingly, the microhardness in the ductility region increases even at low photon treatment doses, thus indicating the onset of crystallization. The diffraction patterns of the samples heated during thermal processing to the crystallization temperature and those irradiated at E_e = 11 J cm^{-2} exhibit more intense reflections in the latter case. This suggests more active crystallization upon photon treatment.

The properties of amorphous alloys in the system Fe–P–Nb [112] are comparable with those of one of the best commercially available alloys, Metglas 2826. Nanocrystallization activated by photon treatment led to improvement of the properties of these amorphous alloys compared to those attained upon thermal processing. An analysis of the X-ray diffraction patterns of the $Fe_{80.5}P_{18.4}Nb_{1.1}$ alloy showed [58] that the alloy is in the amorphous state to E_e = 15 J cm^{-2}, the samples remain ductile and their strength increases by a factor of 1.45. At $E_e > 25$ J cm^{-2}, a complete crystallization occurs (*cf.* $T > 770$ K for thermally processed samples).

The temperature dependences of the internal friction (Q^{-1}) and squared resonance frequency of mechanical oscillations $(f/f_0)^2$ obtained for the initial (amorphous) sample following a known procedure [113] are shown in Fig. 15. At a heating rate of 4 K min^{-1}, Q^{-1} gradually increases (see Fig. 15 *a*). In the temperature range 550–690 K, the internal friction increases to a value of 0.04. In the course of crystallization, the Q^{-1} value

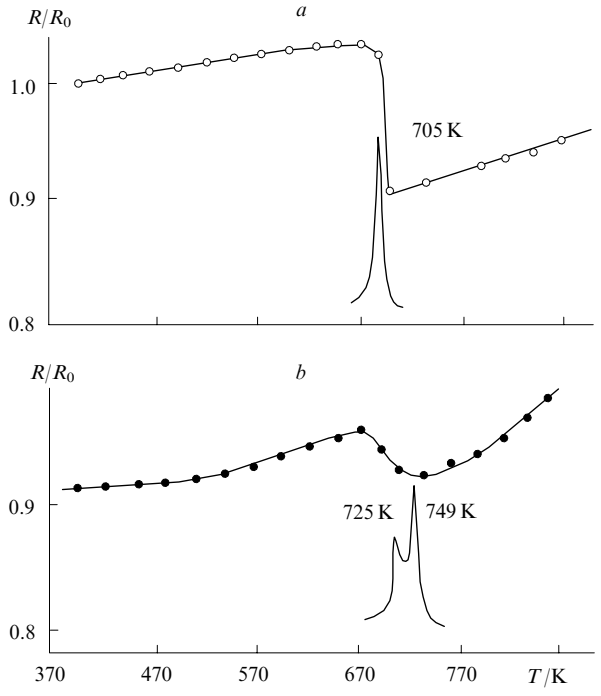


Figure 14. DTA data and the temperature dependence of the resistance of amorphous $Fe_{79.3}P_{18.2}V_{2.5}$ (*a*) and $Fe_{76.8}P_{18.2}V_5$ (*b*).[57] R_0 and R are the initial and running resistance values, respectively.

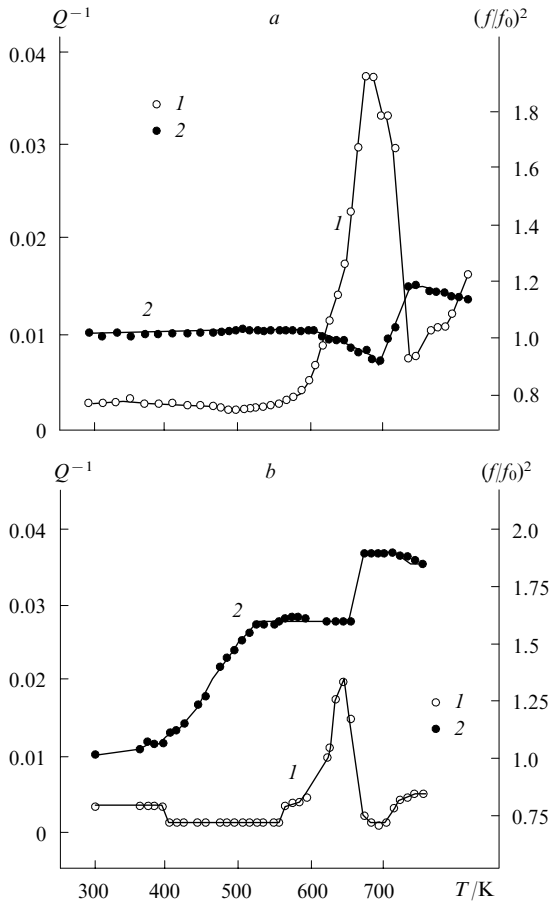


Figure 15. Temperature dependences of internal friction (*1*) and squared resonance frequency of mechanical oscillations (*2*) for untreated samples (*a*) and samples irradiated at 5 J cm^{-2} (*b*).[58]

decreases to 0.008. The relative quantity $(f/f_0)^2$ varies insignificantly in the vicinity of crystallization temperature and increases by about 20% as the alloy goes to the crystalline state. The character of the temperature dependence of Q^{-1} significantly changes for the photon-treated samples (E_e = 5 J cm^{-2}), namely, the $(f/f_0)^2$ value appreciably increases starting with ~400 K (see Fig. 15*b*).

A study[114] of amorphous alloy Fe–Cu–Nb–Si–B revealed a maximum in the temperature dependence of the elastic modulus near the glass transition temperature. The nature of the maximum was associated with the formation of chemical inhomogeneities, or clusters. The elastic modulus of an alloy is proportional to $(f/f_0)^2$; in amorphous state, it is 20%–30% lower than in the crystalline state.[115]

Thus, the effect of preliminary low-dose photon treatment manifests itself in clustering, *i.e.*, nucleation of crystalline phases to be formed and, as a consequence, in strengthening of amorphous alloys upon subsequent thermal heating. Also, the observed influence of photon treatment on crystallization was related[58] to realization of the Franck–Condon principle.[116] Excitation of covalent bonds in amorphous alloys containing glass-forming elements (Si, B, P) violates the equilibrium arrangement of atoms in the vicinity of the atomic pair with the broken bond. A possible model for structural rearrangement is presented in Fig. 16. In the atomic cluster (see Fig. 16*a*), which can be a fragment of the icosahedral structural block of amorphous alloy, cleavage of a covalent bond (see Fig. 16*b*) may lead to transformation of the block to an octahedron (see Fig. 16*c*), a building block of the cubic lattice.

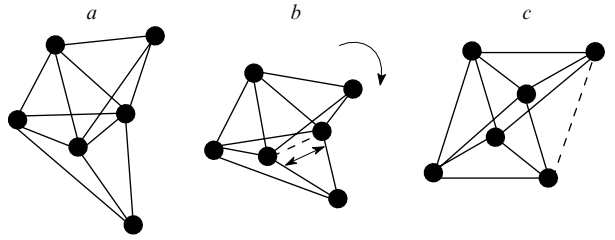


Figure 16. Changes in the structure of amorphous alloy: initial fragment of icosahedral cluster (*a*), after a covalent bond cleavage (*b*), octahedral structural block of a cubic lattice (*c*).[58]

In accordance with the Franck–Condon principle, absorption of a photon causes an instantaneous increase in the potential energy of the excited bond (this increase is of the order of a few tenths of electron-volt), the atomic positions being the same before and after absorption. This potential energy is converted to the kinetic energy of the atoms involved in the formation of the stretched chemical bond and creates a hypersonic wave propagating from the point at which the photon was absorbed. The spread of atomic displacements produced upon absorption of a photon is of the same order of magnitude as the distance between neighbouring atoms and the amplitude of atomic displacements is of the order of a few tenths of the interatomic distance at the photon absorption site. On going from the initiation point, the amplitude rapidly increases; therefore, atomic rearrangement occurs in a relatively small region (to 10 nm in size). Hypersonic wave passing through atomic configurations in which atomic clusters (structural units of the amorphous phase) undergo thermally activated rearrangements to building blocks of crystalline phases favours acceleration of this process. Most nanocrystals will be formed at those sites where the activation energy is minimal. This condition is first of all met in the regions containing the major component. In the experiments, the nanocrystalline phase of the major component is nucleated first and faster.

Propagation of a hypersonic wave from the photon absorption site was analyzed[117–119] within the framework of the model for isotropic elastic medium; also, a mechanism of energy transfer from electrons to phonons was proposed. In particular, a possible model[119] for nonradiative transition of excited electron involves localization of energy within the atomic cluster where the electronic excitation occurs. According to calculations, this mechanism allows the frequency of transition to the ground state to be high enough, being comparable with the optical transition frequencies, and thus influence the kinetics of atomic rearrangements.

V. Synthesis of oxide, nitride and carbide films

Rapid photon treatment of corresponding surfaces in various gas atmospheres makes it possible to carry out oxidation, nitridation or carbidization reactions at much lower thermal loads owing to short irradiation time and the possibility to localize the photon flux energy. This technique is promising for fabrication of dielectric films for microelectronics, opto-electronic devices, memory devices, *etc.* Photon treatment of amorphous films of appropriate elemental composition prepared by different methods enables the synthesis of complex oxides.

Since the photon treatment technique was initially developed to solve problems in microelectronics technology, its applicability to one of the key processes, the synthesis of SiO_2 films, was studied.[8,120] Traditionally, planar technology of formation of dielectric films on single-crystalline silicon involves thermal oxidation in anhydrous or moist oxygen. Although thermal oxide films are characterized by high quality and exhibit high resistivity, electric strength and dielectric constant, thermal oxidation occurring at 1000–1250 °C has some drawbacks (for details, see a monograph[30]). These drawbacks are mainly due to the high temperature and duration of the process. But thin SiO_2 films (thickness 1.5–5.0 nm) can also be synthesized by rapid photon treatment (150 K s^{-1}) at atmospheric pressure of oxygen.[8]

A possible way to reduce the temperature of the process and the thermal load on the heterosystem is to carry out vapour-phase deposition of films of appropriate composition followed by rapid photon treatment which insignificantly influences the structure and properties of thermal SiO_2.[120] This is quite obvious taking into account the optical properties of SiO_2 films formed by vapour-phase deposition. Significant structural transformations occurred upon pulsed irradiation of films prepared by plasma-chemical deposition (pulse duration 1.4–10.0 s); the properties of the films approached those of thermal SiO_2. The response to irradiation is due to a feature of the initial structure of such films and to corresponding optical absorption.

The effect of photon treatment in the course of oxidation was discussed[121] in connection with investigations of (i) experimentally observed optical effect in laser-induced

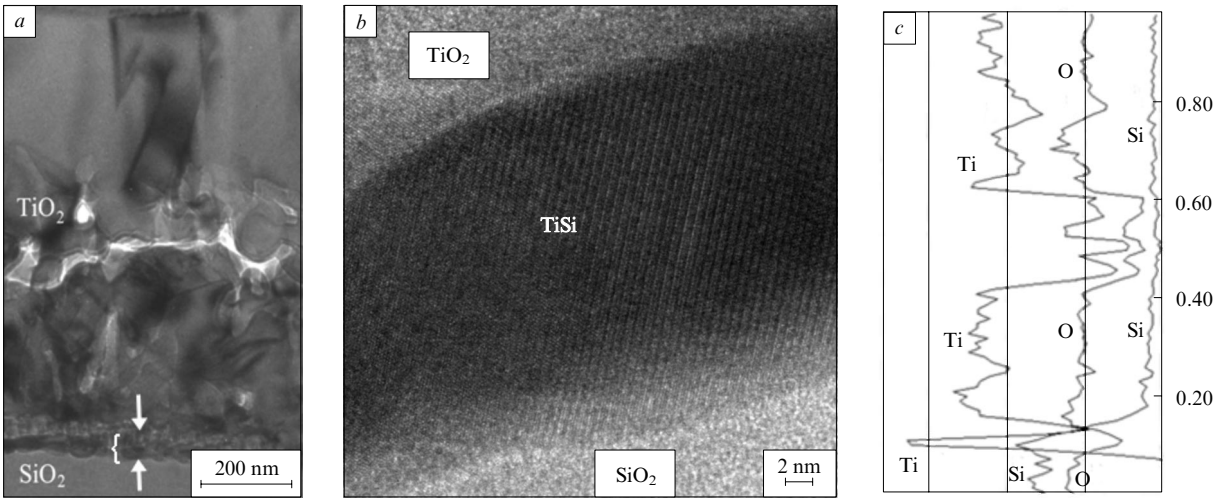


Figure 17. Cross-sectional TEM images of $TiO_2/TiSi/SiO_2$ heterostructure (*a*) and TiSi layer near the interphase boundary (*b*); changes in the *K*-lines in X-ray spectra of components in the region of TiO_2/SiO_2 phase boundary (*c*).[124]
Arrows and a brace in Fig. 17 *a* indicate the silicide region across the thickness of the heterostructure.

thermal oxidation of silicon in the near-IR (1.064 μm) and IR (10.6 μm) regions and (ii) vacuum-UV (157 nm) laser-induced oxidation of silicon at low temperatures.[122] The mechanisms of oxidation were associated with diffusion of molecular ions O_2^- (Ref. 121) and with diffusion of oxygen atomic species O^-.[122] It was concluded[122] that vacuum-UV-laser-induced oxidation of silicon at low temperatures is not related to radiation absorption by silicon, being a result of a photochemical process involving the formation of oxygen atoms or atomic species in the vapour phase. Also, it was shown that ozone is not the main oxidizing agent. This is very important because some authors explained acceleration of the oxidation process by the effect of ozone whose formation accompanies radiation of xenon lamps.

Thin films of TiO_2 are promising for various applications because this material has high dielectric constant and refractive index, is optically transparent in the visible and near-IR regions and demonstrates high chemical and thermal stability. Photon treatment was utilized to both activate the oxidation of titanium[121,123–126] and to crystallize amorphous films of necessary composition (*e.g.*, films prepared by plasma-assisted chemical vapour phase deposition) in the anatase phase or for subsequent transformation to rutile.[31] In the latter case, the initial phase (anatase) dominated in the TiO_2/Si heterostructure until 600 °C. When the heterostructure was irradiated with light of halogen lamps (800 °C, 60 s), its dielectric constant increased to 47.4 at low leakage currents ($< 3 \times 10^{-7}$ A cm^{-2}). It was concluded that photon treatment is a promising technique because it leads to a decrease in the density of defects and excludes the formation of silicides, thus avoiding problems related to the leakage current.

The oxidation of poly- and single-crystalline titanium films under photon treatment with radiation of xenon lamps was studied.[124,125] Untreated films about 0.5 μm thick condensed by electron-beam evaporation on the surface of unheated oxidized silicon wafer have a nanocrystalline substructure with an average grain size of about 30 nm; X-ray diffraction experiments revealed a well-defined ⟨0001⟩ texture. Single-pulse photon treatment was carried out in air. The pulse duration was $\tau = 1.4$ s and the power density varied from 115 to 230 J cm^{-2}.

The oxide film thickness (h) obtained at different power density values was as follows:[124]

E_e /J cm^{-2}	115	145	170	230
h /nm	141	162	305	1012

A comparison of the TEM images of cross-sectional samples of the heterostructures before and after oxidation at $E_e = 230$ J cm^{-2} showed that the process was completed. This was also confirmed by the results of X-ray diffraction study, according to which a mixture of oxides Ti_2O_3 and TiO_2 is formed at $E_e = 170$ J cm^{-2}, whereas only TiO_2 (rutile) was detected at $E_e = 230$ J cm^{-2}.

The TEM image of the cross-sectional sample of $TiO_2/TiSi/SiO_2$ heterostructure is presented in Fig. 17 *a*. The diffraction contrast shows that at a noticeable inhomogeneity of the grain substructure with thickness of the TiO_2 film, the upper part of the oxide layer has a more perfect substructure, while the region near SiO_2 represents a continuous layer of the second phase 20–30 nm thick (arrowed). Correspondence between the boundary phase and the TiSi silicide was substantiated by the results of analysis of the high-resolution image shown in Fig. 17 *b* where the TiSi (001) plane was established and by the distribution of elements with respect to the sample thickness (Fig. 17 *c* demonstrates an abrupt increase in the titanium and silicon content and a decrease in the oxygen content within the boundary layer).

At a power density of 230 J cm^{-2}, the oxidation rate is two orders of magnitude higher than the rate estimate for a linear portion of the kinetic curve for thermal oxidation of massive titanium preforms‡ at 870 °C.[127] Some contribution to acceleration of the process comes from significantly larger proportion of grain boundaries in the film compared to the massive sample of Ti preform. However, a structural

‡ Initial form of the titanium sample being oxidized.

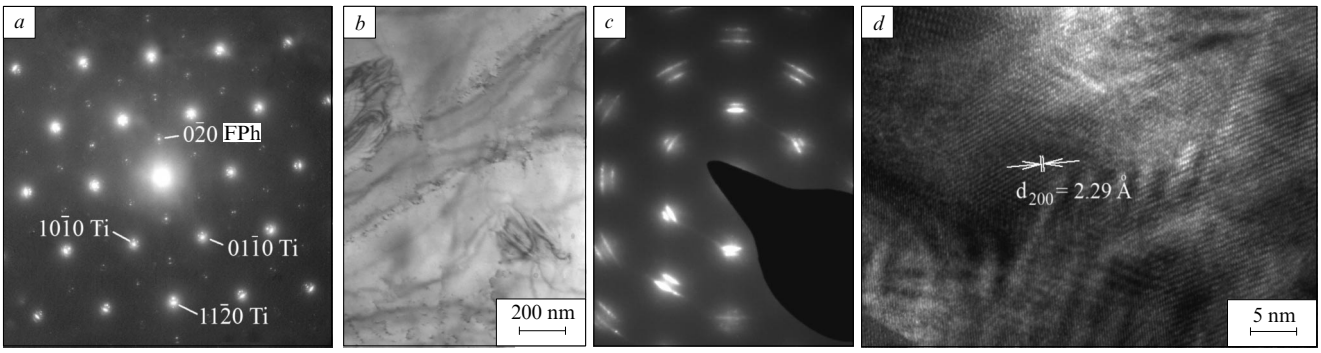


Figure 18. Electron diffraction patterns (*a*, *c*) and TEM images (*b*, *d*) of the single-crystalline titanium film on fluorphlogopite (FPh) before (*a*, *b*) and after photon treatment at 110 J cm^{-2} in air (*c*, *d*).[125]

study of cross-sectional samples showed that recrystallization of the titanium film occurs at E_e = 110 J cm^{-2}, the grain size and subgrain being tenfold larger than the corresponding initial parameters.

The threshold E_e value at which a 50-nm thick single-crystalline titanium film with (0001) orientation on fluorphlogopite (FPh) is oxidized in air to rutile is 95 J cm^{-2} (τ = 1.2 s).[125] The electron diffraction patterns and TEM images of the film treated at E_e = 110 J cm^{-2} (τ = 1.4 s) are shown in Fig. 18. The titanium film undergoes a complete oxidation to rutile in the orientation relationships

$$(010), [101]\ TiO_2 \parallel (0001), [1\bar{1}00], [10\bar{1}0] \text{ and } [0\bar{1}10]\ Ti \qquad (4)$$

Taking into account the twin positions, TiO_2 grains in six azimuthal orientations are formed on the Ti(0001) plane. This predetermines a high degree of dispersion in the grain structure of the oxide (grain and subgrain size reach a value of 30 nm). The orientation and substructure of the film are similar to those of a film obtained by thermal oxidation at 600 °C for 5 min, but the grain structure is characterized by higher degree of dispersion including narrower twins. An increase in E_e to 160 J cm^{-2} (τ = 2.0 s) did not lead to significant structural and phase transformations because of the optical transparency of rutile and substrate for which the band gap is about 3.0 and 5.5 eV, respectively. At the same time, thermal processing of the Ti film/substrate heterostructure at 1000 °C for 5 min led to formation of larger rutile grains (to 0.4 μm in size).

A Ni/SiO_2/single-crystalline Si wafer/SiO_2/Ni heterostructure was fabricated to study the effect of photon activation of the oxidation of nickel films.[128, 129] Untreated nickel films condensed at 473 K had a polycrystalline structure with randomly oriented grains. The heterostructure was irradiated on one side (E_e = 50–250 J cm^{-2}). At $E_e \leqslant$ 140 J cm^{-2}, the thickness of the oxide film on the irradiated side was somewhat larger (by at most 5 nm) than on the back side. At $E_e \geqslant$ 155 J cm^{-2}, the process slowed down. This to a greater extent concerned the irradiated side, but the threshold E_e values corresponding to cessation of the oxide growth were almost the same for both sides. Retardation of growth of the NiO layer on the irradiated surface was related to possible light-induced oxygen desorption[130] taking into account the fact that the bond between oxygen adatoms and the oxide surface is weaker than the bond between oxygen adatoms and the surface of the nickel film.[131] Retardation of the oxidation of titanium and vanadium films upon laser irradiation (1.96 and 3.39 eV, respectively) was explained by transition of oxygen adatoms to the lowest triplet state characterized by low reactivity.[123]

Transparent CdO films exhibit high conductivity and can be used in opto-electronic devices, such as solar cells and photogalvanic devices, flat displays, transparent electrodes, Ohmic contacts with LEDs and reflectors. Various methods of synthesis of CdO films including rapid photo-induced thermal oxidation are studied.[132] For instance, CdO films deposited by pyrolysis of aqueous cadmium nitrate were illuminated with halogen lamps (10 min, 450 °C) in air.[33] The key effects of photon treatment consist in an increase in the grain size, changes in texture, a decrease in the lattice constant and the width of the forbidden gap.

The efficiency of utilizing radiation of gas-discharge lamps in the synthesis of complex oxides was demonstrated.[49–53] The structure and properties of 0.4 μm thick lead zirconate titanate films deposited on the Pt/Si heterostructure by metallo-organic decomposition were compared after thermal processing and photon treatment with radiation of halogen lamps (to 60 s).[49] The effect of photon treatment manifested itself as a more smooth surface, larger grain size and significant increase in the dielectric constant (1200 *vs.* 1400),§ residual polarization (30 *vs.* 35 μC cm^{-2})§ and coercive field (65 *vs.* 85 kV cm^{-1}).§ The structure of lead zirconate titanate films depends on the heating rate, namely, an increase in the heating rate leads to more uniform nucleation of the crystalline phase, more dense microstructure and to improvement of ferroelectric properties.[50]

Photon treatment (800 °C, 1 min) of 0.4-μm-thick $Ba_{0.64}Sr_{0.36}TiO_3$ films prepared by the sol–gel technique was reported.[51] Judging from the properties of the films determined after irradiation, this kind of processing is promising for fabrication of dielectric IR sensors.

A study[52] of the properties of $LiTaO_3$-based films for IR detectors revealed that the pyroelectric and dielectric properties of films prepared by the sol–gel technique depend nonmonotonically on the heating rate in the rapid photon treatment regime (700 °C, 2 min), *viz.*, the optimal

§ The first number is for thermal processing and the second number is for photon treatment.

regime was found to be at 30 K s^{-1} for the overall range from 10 to 50 K s^{-1}.

The effect of photon treatment in the case of solid-phase synthesis of $PbTiO_2$ films was studied.[53] Untreated films 0.4 μm thick had a chemical composition close to $PbTiO_3$ and were deposited by high-frequency magnetron sputtering of ceramic targets of the necessary composition on both sides of nonoxidized and oxidized single-crystalline silicon wafers. Photon treatment involved irradiation of one side of the heterostructure with light of xenon lamps in air. The untreated films were mainly amorphous and contained inclusions of TiO_2 and lead oxide nanoparticles. Photon treatment (90 J cm^{-2}, 1.0 s) produced $BaTiO_3$ on the irradiated side and nearly equal amounts of $PbTiO_3$ and $Pb_2Ti_2O_7$ on the back side. A conventional synthesis of single-phase $PbTiO_3$ films requires thermal processing at 670 °C (20 min).[133] Thus, similarly to the synthesis of metal silicides, the effect of photon treatment consists in acceleration of the synthesis and reduction of the temperature threshold to the formation of the final phase.

Compared to thermal processing, the effect of rapid photon treatment on the synthesis of $LiMn_2O_4$ thin films prepared by deposition from a solution containing lithium and manganese acetates manifests itself as smaller grain size, higher density of the films, more smooth surface relief and better properties of the films as a cathode material.[134]

Transition-metal nitride, oxynitride and carbide films exhibit such practically valuable properties, as high hardness, strength, wear resistance, melting point and chemical stability. Titanium and tantalum nitrides are used as efficient diffusion barriers in microelectronic devices. Utilization of rapid photon treatment in the synthesis of metal nitride thin films may be aimed at:

— irradiating metal films in particular gas atmosphere (ammonia, nitrogen) and

— substrate coating with films of necessary compositions by magnetron sputtering followed by photon treatment to modify the structure and properties of the films.

The main feature of the formation of titanium nitride is as follows: rapid photon treatment (5 s) of the metal film on silicon in nitrogen atmosphere (nitrogen is supplied to the reaction chamber upon creating a vacuum of 10^{-2} Torr) causes the rate of nitride formation to increase by several orders of magnitude compared to the rate attained under long-term thermal processing in nitrogen atmosphere.[135] This suggests the action of additional mechanisms, in particular, formation of nitrogen ions and, therefore, acceleration of their diffusion into the metal.

The results of nitridation of α-Nb(N) thin polycrystalline films on the surface of SiO_2/Si heterostructure under photon treatment with radiation of halogen lamps (800 °C, 60 s) and under thermal processing conditions (900 °C, 24 h) in NH_3 atmosphere were compared.[35] In the former case, poreless single-phase NbN films with smooth surface are formed, whereas in the latter, Nb_5N_6 films with microporous structure. Also, photon treatment activates a reaction resulting in a thin layer of NbO_2 at the interface with SiO_2.

High efficiency of photon treatment with light of halogen lamps was demonstrated in a study on modification of the properties of SiN_x thin films for solar cells, namely, irradiation for 1–3 s led to a 200% increase in the lifetime of minority charge carriers.[37]

Synthesis of tungsten carbide films by magnetron sputtering[136,137] produces a metastable phase β-WC with NaCl-type structure. Transformation to the stable hexagonal α-WC phase requires subsequent heat treatment with heating to 850 °C.

The possibility of synthesis of tungsten carbide films by photoactivated solid-phase reactions in two- (W/C), three- (C/W/C) and twenty-layer heterostructures (W/C...W/C) up to 0.5 μm thick was investigated.[54,138] The initial heterostructures were formed by electron-beam evaporation and vacuum deposition of tungsten and carbon in the desired order on the surface of 380 μm thick oxidized silicon wafers and 30 μm thick tungsten foil. The electron diffraction patterns and TEM images of the initial three-layer heterostructure C/W/C (total thickness is about 0.1 μm) before and after photon treatment are shown in Fig. 19. The untreated heterostructure consists of amorphous carbon films and nanocrystalline tungsten film (average grain size is about 5 nm). The formation of carbide mainly begins with the orthorhombic phase W_2C at $E_e > 170$ J cm^{-2}; at $E_e = 200$ J cm^{-2}, two-phase carbide (W_2C and α-WC) is formed and at $E_e > 300$ J cm^{-2}, single-phase carbide α-WC

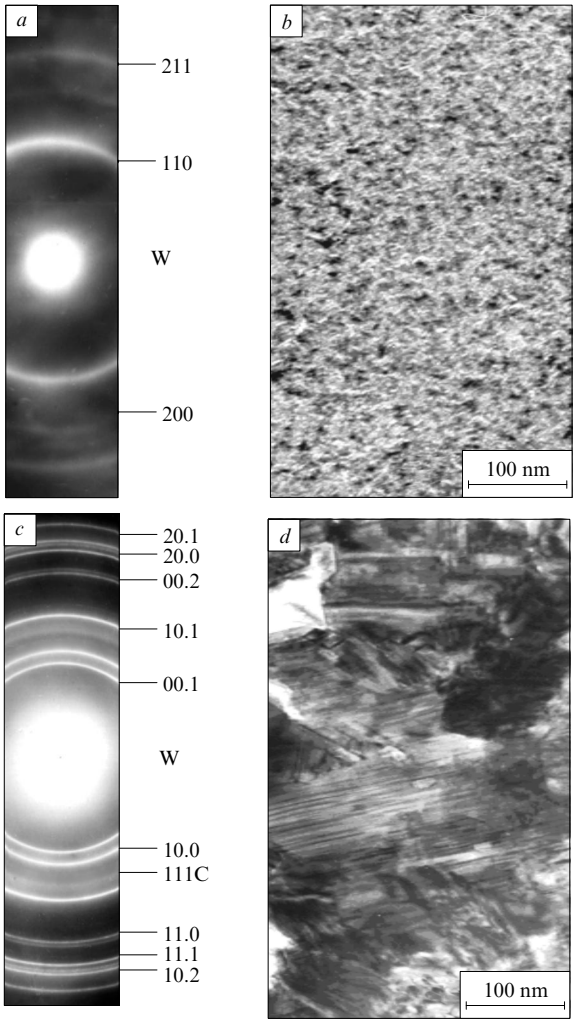


Figure 19. Fragments of electron diffraction patterns and TEM images of C/W/C heterostructure before (*a*, *b*) and after photon treatment at 320 J cm^{-2} (*c*, *d*).[54]

appears. Blocks of the hexagonal phase α-WC are comprised of thin (~10 nm) twin layers and can be as large as 200 nm (see Fig. 19). Thermal processing of an analogous initial heterostructure (1250 °C, 10 s) gave two-phase carbide (W_2C and α-WC). The temperatures attained during photon treatment (2 s) and processing in axial furnace (10 s) were compared and it was shown that in the former case, two-phase carbide is formed at lower temperature (by about 80°). In the latter case, trace amounts of tungsten were detected and the degree of dispersion of the grain substructure was much higher. Also, in the latter case, the early steps of the synthesis of carbide are accompanied by partial oxidation of the metal resulting in WO_3. Photon treatment suppresses the formation of oxide; this is consistent with laser-induced desorption of oxides from the surface of polycrystalline tungsten.[139] The results of X-ray diffraction study of the photon-treated 20-layer heterostructures confirm the general regularity of changes in the threshold E_e values for the formation of carbide phases.

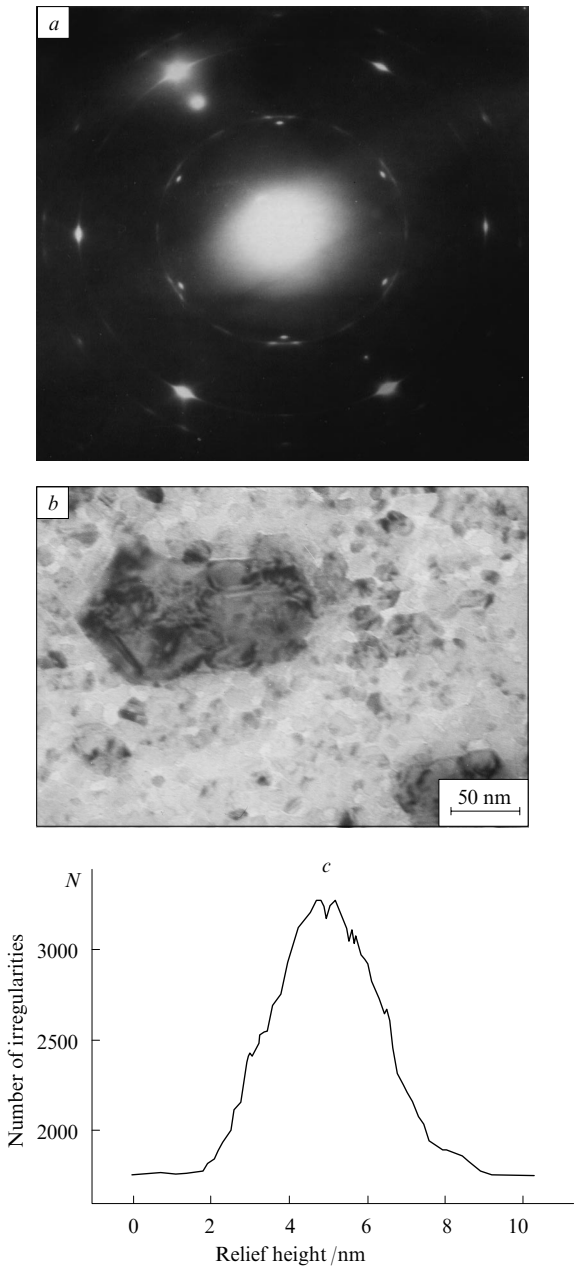


Figure 20. Electron diffraction pattern (*a*), TEM image (*b*) and the height distribution of surface relief for β-SiC film on Si(111) surface (*c*).[140]

An attempt to practically implement epitaxial carbidization of the surface of single-crystalline silicon wafers was reported.[55,140] Photon treatment was carried out in two ways. First, photon treatment (260 J cm^{-2}, 2 s) was used to activate a solid-phase reaction in the 'Si/thin carbon film' heterostructure (the film was deposited by electron-beam evaporation and vacuum condensation). This resulted in continuous β-SiC film with highly dispersed, epitaxial mosaic substructure and a rather smooth surface (Fig. 20). Second, photon treatment of the Si(111) surface was carried out in a $C_3H_8 : C_4H_{10} = 1 : 4$ mixture at a pressure $\sim 10^{-2}$ Pa.[140] It also led to the formation of mosaic nanostructures of the β-SiC film with mainly parallel orientation of the carbide and silicon lattices.

Some other examples illustrating the potential of photon treatment in modification of the free surface and phase boundary are available. For instance, thin (2.5–5.5 nm) gold films on the surface of silicon wafers covered with a native layer of SiO_2 2.5 nm thick were exposed to rapid photon treatment with light of halogen lamps in appropriate regime. This led to disintegration of the films and formation of island structure characterized by a narrow island size distribution (15–25 nm).[141] Utilization of such islands as catalytic sites for growth of filamentary crystals with controlled diameter excludes the use of photolithography and electron–beam lithography.

The effect of photon treatment clearly manifests itself in enhanced bioactivity of a zirconium implant in biomimetic synthesis of hydroxyapatite.[47] Extrinsic photoexcitation at 260–400 nm of the low-coordinated (lc) surface of ZrO_2 anode generated electron–hole pairs comprised of (Zr^{3+}) and oxygen vacancies (O^-) in the reaction

$$(Zr^{4+} - O^{2-})_{lc} + h\nu \longrightarrow (Zr^{3+} - O^-)^*_{lc} \quad (5)$$

The reaction of electron–hole pairs with adsorbed water

$$(Zr^{3+} - O^-)^*_{lc} + H_2O \longrightarrow Zr^{4+} - OH + H_2 \quad (6)$$

resulted in abundant $Zr^{4+} - OH$ groups that act as active sites of nucleation of the hydroxyapatite coating.

Localization of radiation within the hydroxyapatite coating/Ti phase boundary (this is also favoured by sufficiently high optical transparency of the coating) activates solid-phase reactions and eventually leads to improvement of adhesive strength.[59]

VI. Conclusion

Application of rapid photon treatment with broadband radiation of power pulsed xenon lamps is not limited to the examples of solid-phase processes mentioned above. Most publications are concerned with technological problems and comparison of the results obtained with those of isothermal treatment which usually takes a longer time. These estimates only substantiate the fact that in almost all cases, photon treatment has advantages over traditional thermal processing. This first of all concerns acceleration of

the overall technological process which favours the formation of nanostructures and more smooth morphology of the free surface. 'Athermal effect' of photon treatment, *i.e.*, the effect of photon activation of solid-phase processes, manifests itself in reduction of the temperature thresholds to formation of corresponding phases compared to the thermal processing regime.

Based on the available concepts of the mechanism of experimentally observed effect of photon treatment and comparison with traditional thermal processing, it may be concluded that:

— in diffusion-controlled processes, the effect of photon treatment is related to excitation of the electronic subsystem by photons, to an increase in the probability of atom–atom bond cleavage and to an increase in the concentration of vacancies;

— in crystallization of amorphous structures (amorphous metal alloys, complex oxides, semiconductors), when there is no need for long-range diffusion, excitation of the electronic subsystem by photons ensures switching of atom–atom bonds within local regions whose compositions match the stoichiometry of corresponding crystalline phases;

— no systematic studies on the kinetics of processes activated by photon treatment were reported; the state of the art in research on metallic systems still can be described by the phrase 'the interaction of photons with metals in the range 2000–9000 Å receives insufficient attention from experimentalists' (see a monograph [141]).

Taking into account specific features of the properties of metal nanoparticles, namely, large optical absorption cross-sections and high concentration of electromagnetic radiation energy in the vicinity of nanoparticles in regions much smaller than the radiation wavelength, control of the morphology of discrete metallic nanostructures on the surface of dielectrics and semiconductors as well as activation of corresponding reactions seems not to be improbable.

Methodologically, it is appropriate to utilize a feature of second-range photon treatment, *viz.*, the fact that the temperature increases nearly in proportion to time. This may be useful in order to reveal light-induced, temperature-dependent processes and transformations that occur during the relatively short irradiation time and/or immediately follow the irradiation step. Relatively high energy supply rates favour detection of steps corresponding to formation of intermediate phases including metastable ones. The potential of the photon treatment technique in activation of gas-phase processes is not realized, although interesting results concerning the deposition of nanographite from gaseous hydrocarbons are available.[142]

References

1. V A Lobunov, V E Borisenko, D I Zarovskii *Zarubezh. Elektron. Tekh.* **8** 27 (1985)
2. D Levy, A Grob, J J Grob, J P Ponpon *Appl. Phys., A: Mater. Sci. Proc.* **35** 141 (1984)
3. E Ma, B S Lim, M A Nicolet *Appl. Phys., A: Mater. Sci. Proc.* **44** 157 (1987)
4. V M Ievlev, S B Kushchev, V P Zlobin *Fiz. Khim. Obrab. Mater.* (2) 128 (1986)
5. V V Egorov, V P Zlobin, V M Ievlev, S N Korol'kov, M A Mkhitarov, L I Shchukin *Elektron. Prom-st* **35** (2) 6 (1988)
6. C J Lee, Y K Sung *J. Electron. Mater.* **22** 717 (1993)
7. G G Chigir', V A Pilipenko, N I Sterzhanov, in *Vzaimodeistvie Atomnykh Chastits s Tverdym Telom. Materialy Konferentsii* [Interaction of Atomic Particles with Solid. Proceedings of Conference, Pt. 2, Minsk, 1984] p. 94
8. A T Fiory *J. Electron. Mater.* **28** 1358 (1999)
9. W M Paulson, R N Legge, C E Weitzel *J. Electron. Mater.* **16** 187 (1987)
10. M Tamura, K Ohyu *Appl. Phys., A: Mater. Sci. Proc.* **49** 149 (1989)
11. M Fu, V Sarvepalli, R K Singh, C R Abernathy, X Cao, S J Pearton, J A Sekhar *J. Electron. Mater.* **27** 1329 (1998)
12. J H Liang, S C Wang *Nucl. Instrum. Methods Phys. Res., Sect. B* **261** 651 (2007)
13. Y Furuhashi, S Yoshida, D Ozaki, T Inovha *Nucl. Instrum. Methods Phys. Res., Sect. B* **242** 633 (2006)
14. V E Borisenko, V V Gribkovskii, V A Labunov, V A Samuilov, K D Yashin *Phys. Status Solidi, A* **75** 117 (1983)
15. J H Chen, T F Lei, D Landheer, X Wu, J Liu, T S Chao *Electrochem. Solid State Lett.* **10** H302 (2007)
16. R M Jin, J X Lu, H Y Wang, T Feng *Semicond. Photon Technol.* (1) 37 (2005)
17. S Ruffel, I V Mitcell, P J Simpson *Nucl. Instrum. Methods Phys. Res., Sect. B* **242** 591 (2006)
18. I E Tischenko, V P Popov, A B Talochkin, A K Gutakovskii, K S Zhuravlev *Fiz. Tekh. Poluprovodn.* **38** 111 (2004) [a]
19. Z V Dzhibuti, N D Dolidze, G L Eristavi *Zh. Tekhn. Fiz.* **78** (6) 135 (2008) [b]
20. C T Lee, M Y Yeh, C D Tsai, X T Lyu *J. Electron. Mater.* **26** 262 (1997)
21. M Delfino, J G Degroot, K N Ritz, P Muillot *J. Electrochem. Soc.* **136** 215 (1989)
22. Yu A Kapustin, B M Kolokol'nikov, A A Sveshnikov *Fiz. Tekh. Poluprovodn.* **24** 318 (1990) [a]
23. A Merabet *J. Alloys Compd.* **382** 300 (2004)
24. V P Zlobin, V M Ievlev, B A Konstantinov, V V Mineev, M A Mkhitarov, A A Sveshnikov, N N Tonkikh *Elektron. prom-st* **33** (2) 69 (1987)
25. S Vankataraman, R Singh, V Parinar, K F Poole, A Ronatgi, V Veludur, A E Bong *J. Electron. Mater.* **28** 1394 (1999)
26. S T Shishiyanu, T S Shishiyanu, S K Roilyan *Fiz. Tekh. Poluprovodn.* **36** 611 (2002) [a]
27. C-C Wang, Y K Wu, W H Wu, M Ch Chen *Jpn. J. Appl. Phys. Part 1* **44** (1A) 108 (2005)
28. J Chen, D Yang, X Ma, H Li, D Que *J. Appl. Phys.* **101** 033526 (2007)
29. J Chen, D Yang, X Ma, D Que *Appl. Phys., A: Mater. Sci. Proc.* **94** 905 (2009)
30. V A Pilipenko *Bystrye Termoobrabotki v Tekhnologii SBIS* (Quick Thermal Treatment in the Very Large-Scale Integration Technology) (Minsk: Belarusian State University, 2004)
31. I S Lee, J-W Kim, Ch-J Youn, S K Pork, Y-B Hahn *Korean J. Chem. Eng.* **13** 473 (1996)
32. T Bondiar, C S Sandu, B Canut, M G Blanchin, V S Teodorescu, J A Roger *J. Sol-Gel Sci. Technol.* **26** 1067 (2003)
33. R A Ismail *J. Mater. Sci.: Mater. Electron.* **20** 1219 (2009)
34. I Galesic, B O Kolbesen *Fresenius J. Appl. Chem.* **365** 199 (1999)
35. A O Berendes, O Brunkahl, C Angelcort, W Bock, F Hofer, P Warbichler, B O Kolbesen *Anal. Bional. Chem.* **379** 554 (2004)
36. V A Matulitskaya, W Bock, K Thoma, B O Kolbesen *Microchim. Acta* **156** 33 (2007)
37. Y Li, P Luo, Z Zhou, R Cui, J Huang, J Wang *Front. Energy Power Eng. China* **2** 519 (2008)
38. A Ronatgi, P Doshi, A Ebong, S Narasimha, T Krygowski, J Moschner *Bull. Mater. Sci.* **22** 383 (1999)

39. H Ito, T Kusunoki, H Saito, S Ishio *J. Magn. Soc. Jpn.* **27** 1083 (2003)
40. H Miyazaki, R Mikami, A Yamada, M Konagai *Jpn. J. Appl. Phys., Part 1* **43** (7A) 4244 (2004)
41. S Neretina, N V Sochinskii, P Mascher *J. Electron. Mater.* **34** 786 (2005)
42. K Jang, K Lee, J Kim, S Hwang, J Lee, S K Dhungel, S Jung, J Yi *Mater. Sci. Semicond. Proc.* **9** 1137 (2006)
43. O Li, J K Shang *J. Am. Ceram. Soc.* **91** 3167 (2008)
44. F F Lu, T H Lin, Ch H Kao *Jpn. J. Appl. Phys., Part. 1* **43** (7A) 4443 (2004)
45. W K Choi, V Ho, V Ng, Y W Ho, S P Ng, W K Chim *Appl. Phys. Lett.* **86** 143 (2005)
46. R L Harper, J W Han, S Hwang, Y Lansari, N C Giles, J W Cook, J F Sihetzina *J. Vac. Sci. Technol. B* **7** 244 (1989)
47. L Zhang, Y Han *Mater. Sci. Eng., C* **31** 1104 (2011)
48. V M Ievlev, B T Boiko, T K Belonogov, B P Bazovoy *Funct. Mater.* **6** 828 (1999)
49. S Lijuan, S B Krupanidhig, H Haertling *Integr. Ferroelect.* 111 (1992)
50. J Lu, Y Zhang, T Ikehara, T Mihara, R Maeda *IEEE Trans. Ultrason. Ferroelectr. Freg. Contr.* **54** 2548 (2007)
51. L Dong, R Yue, L Liu, X Wang, J Liu, T Ren *Int. J. Infrared Millimeter Waves* **24** 1351 (2003)
52. S L Young, M-Ch Kao, H-Z Chen *J. Electrochem.* **17** 799 (2006)
53. V M Ievlev, Yu A Obvintsev, A I Spirin, O V Serbin, A P Isaenko, B L Agapov *Vestn. VGTU, Ser. Materialovedenie* (1.10) 72 (2001)
54. V M Ievlev, S B Kushchev, O V Serbin, V N Sanin, A P Isaenko, E K Belonogov *Perspekt. Mater.* (3) 5 (2008)
55. V M Ievlev, S B Kushchev, E N Fedorova, in *Strukturnye Osnovy Modifikatsii Materialov. Tezisy Nauchnoi Konferentsii* (Structural Foundations of Modification of Materials. Abstracts of Scientific Conference, Obninsk, 2005) p. 57
56. V V Vavilova, V M Ievlev, A P Isaenko, Yu E Kalinin, Yu K Kovneristyi *Neorg. Mater.* **39** 82 (2003) [c]
57. V V Vavilova, V M Ievlev, Yu K Kovneristyi, N A Palii, O V Serbin, B G Sukhodolov *Neorg. Mater.* **40** 811 (2004) [c]
58. V V Vavilova, V M Ievlev, Yu E Kalinin, S B Kushchev, B M Darinskii, N A Palii, S A Pokazan'eva, L Yu Yudin *Metally* **3** (3) 85 (2011) [d]
59. V M Ievlev, S M Barinov, V I Putlyaev, E K Belonogov, A V Kostyuchenko, in *Materialy IV Vserossiiskoi Konferentsii 'Fiziko-khimicheskie Protsessy v Kondensirovannykh Sredakh i na Mezhfaznykh Granitsakh'* (Proceedings of the IVth Conference 'Physicochemical Processes in Condensed Media and at Interfaces', Voronezh, 2008) Vol. 1, p. 385
60. S Noël, L Ventura, A Sloovi, Y C Muller, B Groch, R Schindler, B Froeschle, T Thiler *J. Electron. Mater.* **27** 1315 (1998)
61. *Spravochnik po Lazeram* (Handbook on Lasers) (Ed. A M Prokhorov) (Moscow: Sov. Radio, 19670
62. O V Serbin, Candidate Thesis in Physical and Mathematical Sciences, Voronezh State Technological University, Voronezh, 2003
63. A Agarwal, H J Gossmann, A T Fiory *J. Electron. Mater.* **28** 1333 (1999)
64. *Polycrystalline Semiconductors: Physical Properties and Applications* (Ed. G Harbeke) (Berlin, New York: Springer, 1985)
65. R Kakoschke, E Bussmann, H Foll *Appl. Phys., A: Mater. Sci. Proc.* **50** 141 (1990)
66. V M Ievlev, S B Kushchev, O V Serbin, V N Sanin, A I Spirin *Vestn. VGTU. Ser. Materialovedenie* (1) 77 (2001)
67. B Nguyenphu, A T Fiory *J. Electron. Mater.* **28** 1376 (1999)
68. Yu P Rainova, A V Barkhotkin, E Tenina *Izv. Vyssh. Ucheb. Zaved., Ser. Elektronika* (4) 59 (1999)
69. I Huang, H H Liu, C C Yu *Korean J. Chem. Eng.* **17** (1) 111 (2000)
70. J Niess, C Grunwald, R Strohmaier, Z Nényei *J. Electron. Mater.* **27** 1286 (1998)
71. L F Drummeter Jr, G Hass, in *Physics of Thin Films* (Eds G Hass, R Thun) (New York: Academic Press, 1964)
72. V M Ievlev, O V Serbin, S B Kushchev, V N Sanin, A P Isaenko *Vestn. VGTU, Ser. Materialovedenie* (1.11) 87 (2002)
73. Patent RF 2109362 (1998)
74. Patent RF 2123738 (1998)
75. H-J Erust, F Hurra, L Douillar *Science* **279** 679 (1998)
76. V E Borisenko *Tverdofaznye Protsessy v Poluprovodnikakh pri Impul'snom Nagreve* (Solid-phase Processes in Semiconductors During Pulse Heating) (Minsk: Nauka i Tekhnika, 1992)
77. V M Anishchik, V A Gorushko, V A Pilipenko, V N Ponomarev *Fizicheskie Osnovy Bystroi Termoobrabotki. Otzhig Polikristallicheskogo Kremniya, Dielektricheskikh Plenok, Ochistka Poverkhnosti i Epitaksiya* (Physical Foundations of Quick Thermal Treatment. Annealing of Polycrystalline Silicon, Dielectric Films, Surface Cleaning and Epitaxy) (Minsk: Belarusian State University, 2002)
78. K N Tu, J W Mayer *Thin Films, Interdiffusion and Reactions* (New York: Wiley, 1978)
79. S P Murarka *Silicides for VLSK Applications* (New York: Academic Press, 1983)
80. K A Jackson, V Schreter *Encyclopaedia of Semiconductor Materials Technology* Vol. 2 (Weinheim: Wiley-VCH, 2001)
81. V P Zlobin, V M Ievlev, B A Konstantinov, S N Korol'kov, S B Kushchev, M A Mkhitarov *Elektron. Prom-st'* (2) 165 (1987)
82. V Yu Balashova, Candidate Thesis in Physical and Mathematical Sciences, Voronezh State Technological University, Voronezh, 1999
83. S B Kushchev, Doctoral Thesis in Physical and Mathematical Sciences, Voronezh State Technological University, Voronezh, 2000
84. V M Ievlev, S B Kushchev, S A Soldatenko, A Ya Isaev, V I Rubtsov *Neorg. Mater.* **37** 1256 (2001) [c]
85. P Rosser, G Tomkins *Vacuum* **35** 419 (1985)
86. V M Ievlev, S A Soldatenko, S B Kushchev, Yu V Gorozhankin *Neorg. Mater.* **44** 808 (2008) [c]
87. E I Tochitskii *Kristallizatsiya i Termoobrabotka Tonkikh Plenok* (Crystallization and Thermal Treatment of Thin Films) (Minsk: Nauka i Tekhnika, 1976)
88. T Sawada, S V Pai, S S Lau, D B Poker, C Buchal *J. Mater. Res.* **1** 322 (1986)
89. M I Markevich, A M Chaplanov, V A Mukha *Fiz. Khim. Obrab. Mater.* (4) 27 (1986)
90. M I Markevich, E I Tochitskii, A M Chaplanov *Fiz. Khim. Obrab. Mater.* (6) 92 (1987)
91. M I Markevich *Dokl. NAN Belorusi* **43** (6) 108 (1999)
92. V V Sviridov, Doctoral Thesis in Physical and Mathematical Sciences, Voronezh State Technological University, Voronezh, 1992
93. V I Belyavskii, Yu A Kapustin, V V Sviridov *Fiz. Tekh. Poluprovodn.* **25** 1204 (1991) [a]
94. V S Vavilov, A E Kiv, O R Niyazova *Mekhanizmy Obrazovaniya i Migratsii Defektov v Poluprovodnikakh* (Mechanisms of Defect Formation and Migration in Semiconductors) (Moscow: Nauka, 1981)
95. M I Markevich *Neorg. Mater.* **36** 825 (2000) [c]
96. A M Chaplanov, M I Markevich *Neorg. Mater.* **39** 1 (2003) [c]
97. M I Markevich, Doctoral Thesis in Physical Mathematical Sciences, Belarussian State University, Minsk, 2004
98. V V Egorov, V P Zlobin, V M Ievlev, A N Kastryulev, S B Kushchev, A A Sveshnikov *Elektron. Prom-st'* (9) 2 (1989)
99. V M Ievlev, T L Turaeva, A N Latyshev, A A Sinelnikov, V N Selivanov *Phys. Met. Metallugr.* **103** (1) 58 (2007)

100. B S Bokshtein, Ch V Kopetskii, L S Shvindlerman *Termodinamika i Kinetika Granits Zeren v Metallakh* (Thermodynamics and Kinetics of Grain Boundary in Metals) (Moscow: Metallurgiya, 1986)
101. E S Medvedev, V I Osherov *Teoriya Bezyzluchatel'nykh Perekhodov v Mnogoatomnykh Molekulakh* (The Theory of Nonradiative Transitions in Polyatomic Molecules) (Moscow: Nauka, 1983)
102. V A Kovarskii *Kinetika Bezyzluchatel'nykh Protsessov* (Kinetics of Nonradiative Processes) (Kishinev: Izd. Akad. Nauk Mold.SSR, 1968)
103. L D Landau, E M Lifshits *Kvantovaya Mekhanika* (Quantum Mechanics) (Moscow: Izd. Fiz.-Mat. Lit., 1963)
104. D I Tetel'baum, V Ya Bayankin *Priroda* (4) 9 (2005)
105. D I Tetelbaum, A Y Azov, E V Kurilchik, V V Bayankin, F Z Gilmutdinov, Y A Mendeleva *Vacuum* **70** 169 (2003)
106. D I Tetel'baum, E V Kuril'chik, A Yu Azov *Poverkhnost'. Rentgen., Sinkhrotron. Neitron. Issledv.* (4) 67 (2003) [e]
107. D I Tetel'baum, A Yu Mendeleeva *Pis'ma Zh. Tekh. Fiz.* **30** (11) 65 (2004) [e]
108. V L Levushkin, G P Pokhil, D I Tetel'baum *Poverkhnost'. Rentgen., Sinkhrotron. Neitron. Issledov.* (3) 80 (2012)
109. A B Gerasimov, A P Bibilashvili, Z G Bokhochadze, M T Vepkhvadze, D A Kiliridze, Z Sh Kushitashvili, Z D Samadashvili *Fiz. Khim. Obrab. Mater.* (6) 63 (2001)
110. V V Braun, V V Vavilova, V M Ievlev, Yu E Kalinin, Yu K Kovneristyi, N A Palii, A V Perov, O V Serbin *Neorg. Mater.* **41** 823 (2005) [c]
111. O K Belousov, V V Vavilova, V M Ievlev, Yu E Kalinin, S B Kushchev, N A Palii, S A Pokazan'eva *Neorg. Mater.* **45** 941 (2009) [c]
112. R M Babaeva, V V Vavilova, Yu K Kovneristyi *Dokl. Akad. Nauk SSSR* **304** 139 (1989) [g]
113. V K Belonogov, I V Zolotukhin, V M Ievlev, V S Postnikov *Fiz. Khim. Obrab. Mater.* (5) 61 (1968)
114. E Bonnetti, L Del Biancol, P Allipi, P Tiberto *J. Magn. Magn. Mater.* **140** 477 (1995)
115. I V Zolotukhin, Yu E Kalinin *Fiz. Tv. Tela* **37** 536 (1995) [h]
116. W Harrison *Solid State Theory* (New York: McGraw-Hill, 1970)
117. L Yu Yudin, Candidate Thesis in Physical and Mathematical Sciences, Voronezh State University, Voronezh 2012
118. B M Darinskii, L Yu Yudin *Izv. Akad. Nauk, Ser. Fiz.* **74** 1355 (2010) [i]
119. B M Darinskii, L Yu Yudin *Izv. Akad. Nauk, Ser. Fiz.* **75** 1390 (2011) [i]
120. V A Gorushko, A Z Nikolaenya, V A Pilipenko, V I Sterzhanov, G G Chigir' *Vestn. Bel. Gos. Univ., Ser. 1* (2) 17 (1985)
121. A M Khoviv *Kondens. Sredy Mezhfaz. Granitsy* **1** 58 (1999)
122. A V Osipov, P Patzner, P Hess *Appl. Phys., A: Mater. Sci. Proc.* **82** 275 (2006)
123. A M Chaplanov, A N Shibko *Kvant. Elektron.* **20** 191 (1993) [j]
124. V M Ievlev, S V Kannykin, S B Kushchev, A A Sinel'nikov, S A Soldatenko *Fiz. Khim. Obrab. Mater.* (4) 18 (2011)
125. A A Sinel'nikov, Candidate Thesis in Physical Mathematical Sciences, Voronezh State Technological University, Voronezh, 2011
126. Patent RF 2436727 (2011)
127. K A Solntsev, K A Shashkeev, in *Institut Metallurgii i Materialovedeniya im. A A Baikova RAN — 70 Let. Sbornik Nauchnykh Trudov* (A A Baikov Institute of Metallurgy and Materials Science, Russian Academy of Sciences — 70th Anniversary. Collected Scientific Works (Ed. K A Solntsev) (Moscow: Nauka, 2008)
128. S B Kushchev, S V Kannykin, in *Materialy 6-i Mezhdunarodnoi Konferentsii 'Vzaimodeistvie Izluchenii s Tverdym Telom'* (Proceedings of the Sixth International Conference 'Interaction of Radiations with Solids', Minsk, 2005) p. 310
129. S V Kannykin, Candidate Thesis in Physical Mathematical Sciences, Voronezh State Technological University, Voronezh, 2007
130. A M Khoviv, V A Logacheva, O V Novikov *Vestn. VGU, Ser. Khim., Biol., Farmatsiya* (1) 101 (2004)
131. *Okislenie Metallov* (Oxidation of Metals) Vol. 1 (Ed. J Bonar) (Moscow: Metallurgiya, 1967)
132. R Ismail, O Abdulrazaq *Sol. Energy Mater. Sol. Cells* **91** 903 (2007)
133. L N Korotkov, S A Konstantinov, Yu V Barmin, I V Babkina, A V Bondarev, V V Posmet'ev, S N Kozhukhar' *Pis'ma Zh. Tech. Fiz.* **28** (20) 22 (2002) [f]
134. X Wu, M Ma, Z Xiao, Z He, J Liu, M Xu *J. Mater. Sci. Technol.* **22** 349 (2006)
135. V V Panaryada, V M Anishchik, V A Pilipenko, I V Pilipenko, in *Materialy 8-i Mezhdunarodnoi Nauchno-prakticheskoi Konferentsii 'Aktual'nye Problemy Tverdotel'noi Elektroniki', PEM-2002* (Proceedings of the Eighth International Scientific and Practical Conference 'Topical Problems of Solid Electronics, PEM-2002, Taganrog, 2002) p. 94
136. E A Sobol', O V Sobol', A T Pugachev, A A Podtelezhnikov, in *Almaznye Plenki i Plenki Rodstvennykh Materialov. Sbornik Dokladov na 12-om Mezhdunarodnom Simpoziume 'Tonkie Plenki v Elektronike', ISTFE-12* (Diamond Films and Related Material Films. Proceedings of the XIIth International Symposium 'Thin Films in Electronics', ISTFE-12, Khar'kov, 2001) p. 326
137. E A Sobol', O V Sobol', A T Pugachev, A A Podtelezhnikov, in *Almaznye Plenki i Plenki Rodstvennykh Materialov. Sbornik Dokladov na 12-om Mezhdunarodnom Simpoziume 'Tonkie Plenki v Elektronike', ISTFE-12* (Diamond Films and Related Material Films. Proceedings of the XIIth International Symposium 'Thin Films in Electronics', ISTFE-12, Khar'kov, 2001) p. 330
138. Cs Beleznai, D Vouagner, J P Girardeau-Montaut, L Nvnai *Appl. Surf. Sci.* **138–139** 512 (1999)
139. V M Ievlev, E K Belonogov, V S Il'in, S B Kushchev, S A Soldatenko, A N Lukin *Poverkhnost'. Rentgen., Sinkhrotron. Neitron. Issledv.* (10) 48 (2009) [e]
140. Yu M Litvin, A I Klimovskaya, A S Oberemok, P M Litvin, A A Stadnik, A T Voroshchenko, in *Aktual'nye Problemy Fiziki Tverdogo Tela. Sbornik Dokladov na Mezhdunarodnoi Nauchnoi Konferentsii FTT-2009* ('Topical Problems of Solid State Physics. Collection of Reports on International Scientific Conference, Minsk 2009) Vol. 2
141. R Weiss *Solid State Physics for Metallurgists* (Reading, MA: Pergamon Press, 1963)
142. V M Ievlev, in *Tret'ya Vserossiiskaya Konferentsiya po Nanomaterialam NANO-2009. Tezisy Dokladov* (The Third All-Russian Conference on Nanomaterials NANO-2009, Ekaterinburg, 2009) p. 8

[a] — *Semiconductors (Engl. Transl.)*
[b] — *J. Tech. Phys. (Engl. Transl.)*
[c] — *Inorg. Mater. (Engl. Transl.)*
[d] — *Russ. Metallurgy (Engl. Transl.)*
[e] — *J. Surf. Invest. X-Ray Synchrotron Neutron Tech. (Engl. Transl.)*
[f] — *J. Tech. Phys. Lett. (Engl. Transl.)*
[g] — *Dokl. Phys. Chem. (Engl. Transl.)*
[i] — *Bull. Russ. Acad. Sci., Phys. (Engl. Transl.)*
[j] — *Quamt. Electron. (Engl. Transl.)*
[k] — *Inorg. Mater.: Appl. Res. (Engl. Transl.)*